Article
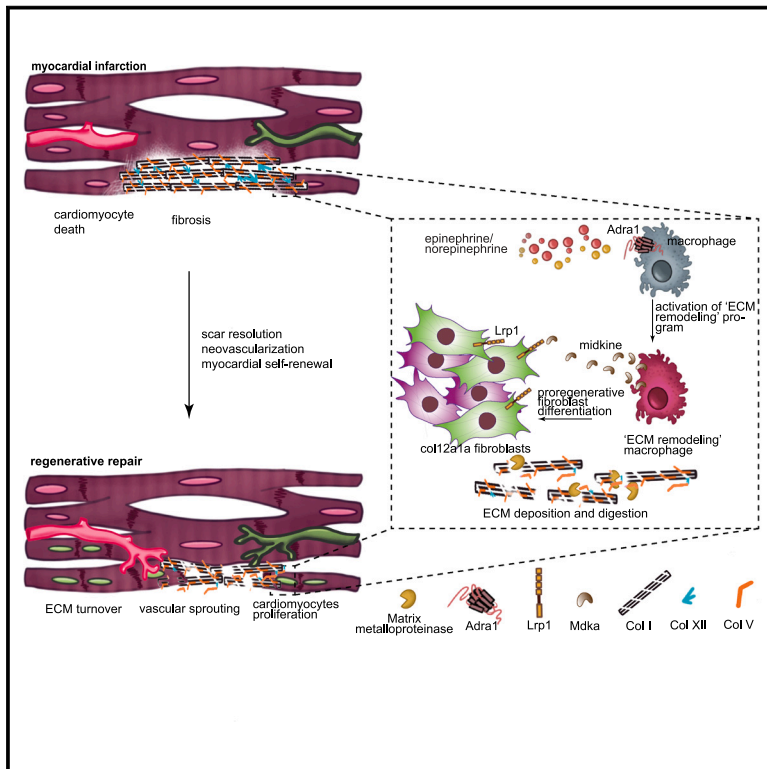
Alpha-1 adrenergic signaling drives cardiac regeneration via extracellular matrix remodeling transcriptional program in zebrafish macrophages

Graphical abstract

Authors

Onur Apaydin, Akerke Altaikyzy,
Alessandro Filosa,
Suphansa Sawamiphak

Correspondence

suphansa.sawamiphak@mdc-berlin.de

In brief

Apaydin et al. identify a mechanism by which the nervous and immune systems orchestrate scarless zebrafish heart repair. They show that a subset of macrophages differentiates in response to neural input through the adrenergic receptor Adra1 to regulate resolution of collagenous scar and allow vascular and cardiac muscle regrowth.

Highlights

- A neuro-immune crosstalk mediated by Adra1 is critical for cardiac regeneration

- Adra1 signals activation of a fibrotic transcriptional program in macrophages

- Activation of proregenerative fibroblasts depends on macrophage Adra1 signaling

- Adra1-activated macrophages promote scar turnover and regenerative microenvironment

CellPress

Article

Alpha-1 adrenergic signaling drives cardiac regeneration via extracellular matrix remodeling transcriptional program in zebrafish macrophages

Onur Apaydin,[1,2] Akerke Altaikyzy,[1] Alessandro Filosa,[1] and Suphansa Sawamiphak[1,3,*]

[1]Max Delbrück Center for Molecular Medicine in the Helmholtz Association (MDC), Berlin, Germany
[2]Institute of Chemistry and Biochemistry, Department of Biology, Chemistry and Pharmacy, Freie Universität Berlin, Berlin, Germany
[3]Lead contact
*Correspondence: suphansa.sawamiphak@mdc-berlin.de
https://doi.org/10.1016/j.devcel.2023.09.011

SUMMARY

The autonomic nervous system plays a pivotal role in cardiac repair. Here, we describe the mechanistic underpinning of adrenergic signaling in fibrotic and regenerative response of the heart to be dependent on immunomodulation. A pharmacological approach identified adrenergic receptor alpha-1 as a key regulator of macrophage phenotypic diversification following myocardial damage in zebrafish. Genetic manipulation and single-cell transcriptomics showed that the receptor signals activation of an "extracellular matrix remodeling" transcriptional program in a macrophage subset, which serves as a key regulator of matrix composition and turnover. Mechanistically, adrenergic receptor alpha-1-activated macrophages determine activation of collagen-12-expressing fibroblasts, a cellular determinant of cardiac regenerative niche, through midkine-mediated paracrine crosstalk, allowing lymphatic and blood vessel growth and cardiomyocyte proliferation at the lesion site. These findings identify the mechanism of adrenergic signaling in macrophage phenotypic and functional determination and highlight the potential of neural modulation for regulation of fibrosis and coordination of myocardial regenerative response.

INTRODUCTION

Ischemic heart disease has long been a leading cause of mortality and morbidity worldwide.[1–3] Currently available treatments fall short to tackle the cause of the problem, namely irreversible loss of cardiomyocytes. Myocardial necrosis provokes acute inflammation and subsequently activation of fibroblasts to deposit collagen-rich fibrotic tissue.[4] Self-renewal capacity of the human heart, like most mammals, is inadequate to replenish the injured myocardium.[5] As a result, permanent non-contractile fibrotic scars weaken cardiac contractility and often lead to heart failure.[6] Clinical efforts, focusing mainly on cell-based approaches attempting to remuscularize infarcted hearts with exogenous cardiomyocytes derived from different types of stem and progenitor cells, have shown minimal cardioprotective effect.[3,7] In neonatal mammals and several non-mammalian vertebrates, the hearts are capable of spontaneous regeneration following apical resection and ischemic myocardial infarction.[8–11] Scar tissue laid down to aid timely recovery of mechanical support and prevention of myocardial wall rupture in the early post-infarct period progressively regresses and is replaced by newly formed cardiac tissue,[11–15] at least in part through inactivation of a profibrotic program in fibroblasts.[15] In light of these insights into the intrinsic regenerative mechanism, an effective therapeutic strategy must not only promote replacement of lost cardiomyocytes but also regulate fibrotic response to prevent excessive scar deposition and enable timely scar regression. The cardiac microenvironment, determined by the inflammatory response post injury, plays a crucial role here.[16]

Macrophages are key inflammatory mediators integral to both scarring and regenerative repair. In an earlier observation, influx of cells into the necrotic heart, although essential to clear out dead cells, is deleterious to cardiac repair and functional recovery as it releases reactive oxygen species and other inflammatory molecules.[17,18] The requirement of macrophages in regenerative repair was later shown when myocardial replenishment was blocked and persistent scarring was induced following macrophage ablation in neonatal mouse, zebrafish, and salamander hearts.[14,19,20] The presence of phenotypically distinct monocyte/macrophage subsets exerting divergent roles in cardiac repair has emerged.[21–31] Macrophage phenotypic heterogeneity similar to the one present in mammals has been demonstrated in the regenerating zebrafish heart.[32–34] Pro-inflammatory *tnfa*+ macrophages are predominant in the heart immediately after injury and promote scar deposition.[33] Subsequent resolution of the inflammation, characterized by a reduction of *tnfa*+ macrophages, correlates with scar removal.[33] In addition to their well-known role in activation of myofibroblast differentiation,[35,36] a subset of macrophages can contribute to fibrosis by directly depositing collagen at the injury site,[34] as

observed in zebrafish and adult mouse hearts. Collectively, heterogeneous macrophage populations, residing in or recruited to the heart upon injury, and existing as a spectrum of activation states, play major roles in both pro- and anti-regenerative cellular events. Interventions to temporally and spatially regulate macrophage phenotypes and harness functionalities of different macrophage subsets to coordinate inflammation resolution, scar regression, and vascular and myocardial regrowth could have a major impact in cardiac regenerative medicine. However, mechanistic underpinnings of the regenerative roles of different macrophage subsets, and the factors driving their functional diversification in the heart, remain largely unknown.

The nervous system plays fundamental roles in maintenance of immune homeostasis and resolution of inflammation. Sensory neurons innervating peripheral organs monitor immune state and communicate the immune signal to the central nervous system (CNS), which, in turn, initiates responses to prevent immune dysregulation and excessive or chronic inflammation through regulation of cytokine production by immune cells within the lymphoid organs.[37–40] Macrophages are among the primary targets of neural control of inflammation.[37,41,42] Involvement of neuronal signals enables faster and more efficient responses to local environmental changes in a specific tissue as compared with humoral or cytokine pathways, which rely mainly on delivery of inflammatory mediators through the circulatory system.[41] Intriguingly, chemical sympathectomy or mechanical vagotomy impairs scarless repair of neonatal mouse hearts, highlighting the importance of the sympathetic and parasympathetic nervous systems in the regenerative process.[43,44] Analyses of transcriptional changes in injured neonatal mouse and zebrafish hearts has implicated blunt innate immune response upon cholinergic inhibition.[44] Insight into the cellular and molecular mechanisms underlying this emerging role of neuro-immune interactions in cardiac regeneration may bridge the gap in our knowledge of the regulation of macrophage activation fundamental to drive the transition from a profibrotic to a proregenerative cardiac environment.

Here, we identified a neuro-immune crosstalk mediated by macrophage cell-autonomous alpha 1-adrenergic signaling as a key regulator of cardiac regeneration, at least in part through the activation of a macrophage transcriptional program characterized by upregulation of extracellular matrix (ECM) proteins and matrix modifying enzyme. Adrenergic stimulation of macrophages promotes remodeling of the collagenous matrix in the lesioned myocardium and regulation of fibroblast activation. These findings enrich our knowledge of macrophage functional diversity and shed more light on the mechanisms of transient fibrotic scar formation. The signaling cascade identified here represents a mechanism by which the nervous and immune systems communicate and orchestrate scarless repair of the damaged myocardium.

RESULTS

Pharmacological inhibition of α1 adrenergic receptor signaling impairs cardiomyocyte and macrophage regenerative response to laser-induced necrosis of the zebrafish larval heart

To first identify neurotransmitter receptors critical for cardiac regeneration and macrophage functional regulation, we used a two-photon laser to induce focal injury to the ventricle of 7-days-post-fertilization (dpf) *myl7:H2B-GFP* zebrafish larvae in which cardiomyocyte nuclei were fluorescently labeled with GFP. This approach permits the precisely localized and highly reproducible cardiac injury most suitable for pharmacological screening. Following injury, we treated larvae with different sympathetic and parasympathetic neurotransmitter blockers for 24 h and measured cardiomyocyte mitotic rate by 16 h 5-ethynyl-2'-doexyuridine (EdU) pulse labeling. Blockage of adrenergic signaling with carvedilol, a non-selective antagonist for α1, β1, and β2 adrenoreceptors, reduced mitotic activity of the injured myocardium as compared with control treatment (Figures 1A and 1B). Efficacy of carvedilol to block α1 receptor in zebrafish was confirmed by diminished methoxamine-mediated α1 receptor activation, measurable by enzyme-linked immunosorbent assay (ELISA) of inositol triphosphate (IP3), a key secondary messenger (Figure S1A). The β-blocker propranolol and the α1-blocker prazosin similarly impaired the post-injury proliferative response of cardiomyocytes (Figures 1A, 1C, and 1D). Blockage of muscarinic receptor signaling with atropine also decreased cardiomyocyte proliferation, although to a lesser extent (Figures 1A and 1E). Interestingly, inhibition of adrenergic and cholinergic transmission differentially affected the response of macrophages to injury. 24 h after laser-induced cardiac necrosis in 7 dpf *myl7:H2B-GFP; csf1ra:Gal4; UAS:NTR-mCherry* larvae expressing GFP in cardiomyocytes and NTR-mCherry in macrophages, non-selective, β-adrenergic, or α1- adrenergic inhibitors, but not muscarinic transmission blockage, effectively inhibited recruitment of macrophages to the injured myocardium (Figures 1F–1J). Macrophage proliferation, by contrast, was unaffected by the treatment (Figures S1B and S1C). Thus, adrenergic signaling plays a primary role in macrophage response to injury and myocardial regenerative repair. Next, we investigated the crosstalk between these processes and tested whether and how macrophages mediate the influence of the adrenergic signal on cardiac regeneration.

Cell-autonomous Adra1 signaling determines macrophage polarization in larval cardiac repair

β adrenergic signaling plays a main role in the regulation of heart contractility, while α1 adrenergic signaling appears not to have major cardiac functions under normal physiological condition.[45] α1 adrenergic signaling thus presents a more attractive target as compared with β adrenergic signaling for the development of an immune modulation strategy to promote cardiac regeneration. To elucidate the macrophage-mediated regenerative function of α1-adrenergic signaling, we generated a new transgenic line to enable macrophage-specific expression of the receptor third intracellular (3i) loop, the segment critical for binding of the receptor to G proteins.[46] This approach was previously employed to efficiently inhibit the signaling pathway downstream of the receptor in a dominant negative manner, through a mechanism that may involve an interaction between the 3i loop and the intracellular domain of the parent receptor, keeping the receptor in an inactive conformation and thereby producing a receptor-specific inhibition.[46–48] Three subtypes of adrenergic α1 receptor—α1A, 1B, and 1D—are $G_{q/11}$-coupled receptors typically signaling via activation of phospholipase C (PLC), which thereby increases IP3 and intracellular Ca^{2+} concentration.[49] Among the five
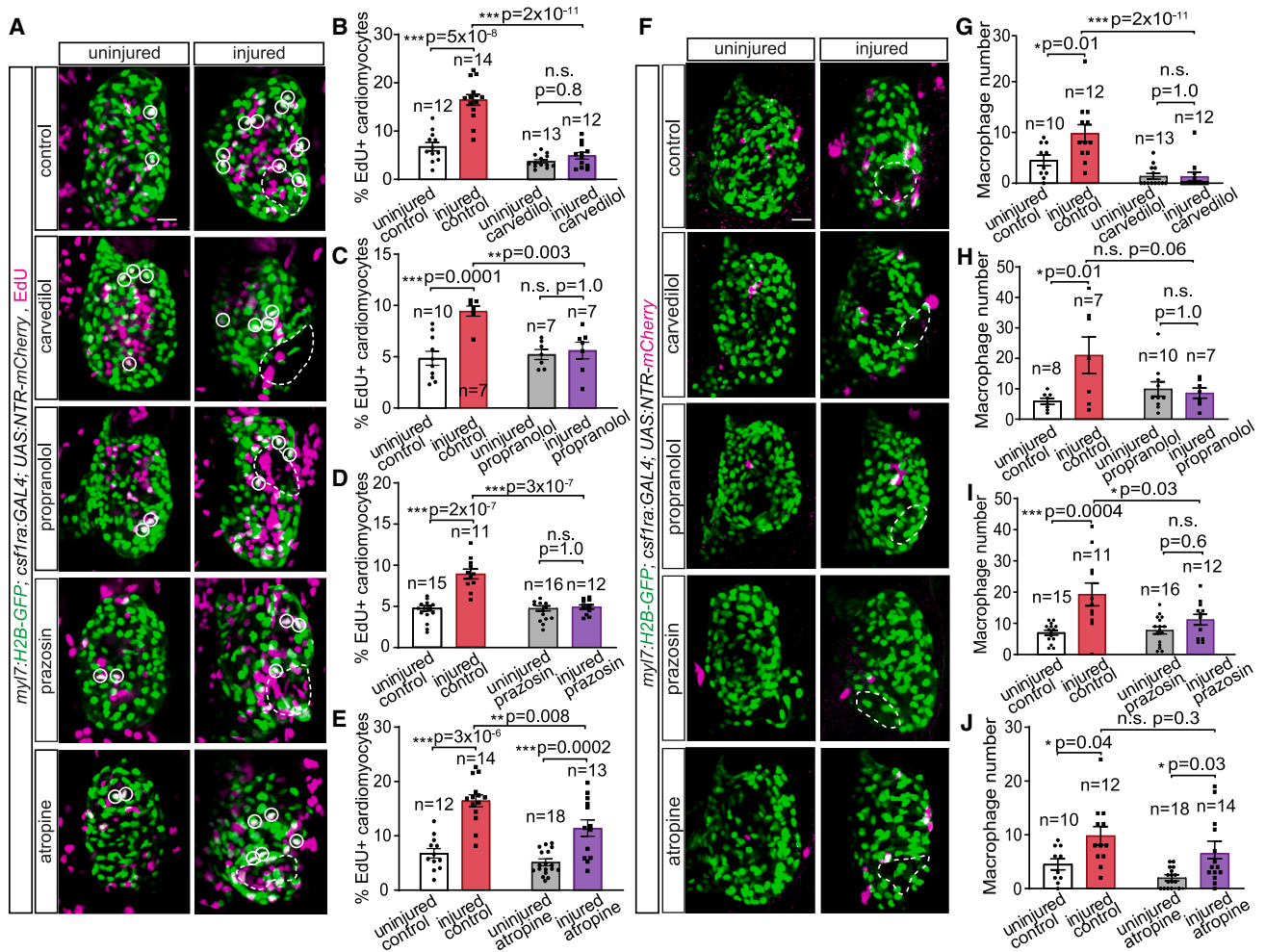
Figure 1. Alpha 1-adrenergic receptor signaling is a key regulator of cardiomyocyte and macrophage response to cardiac injury

(A) 7 dpf *myl7:H2B-GFP*; *csf1ra:Gal4*; *UAS:NTR-mCherry* larvae in which the cardiac ventricles were injured focally with a two-photon laser, and uninjured siblings, after 24 h application of carvedilol, propranolol, prazosin, atropine, or control solution. 16 h EdU pulse-labeled cells undergoing DNA synthesis are in magenta. Cardiomyocytes and macrophages were immunostained with GFP and mCherry, respectively. EdU and GFP channels of the composite images are shown here. Dashed lines outline injury areas. White circles mark proliferating cardiomyocytes.

(B–E) Bar graphs depicting percentages of EdU⁺ cardiomyocytes in the cardiac ventricles of carvedilol-treated (B), propranolol-treated (C), prazosin-treated (D), and atropine-treated (E) groups.

(F) Uninjured and two-photon-injured cardiac ventricles of 7 dpf *myl7:H2B-GFP*; *csf1ra:Gal4*; *UAS:NTR-mCherry* larvae from the same experiment as in (A)–(E) showing GFP and mCherry channels of the composite images. Dashed lines outline injury areas.

(G–J) Bar graphs depicting numbers of macrophages recruited to the ventricle of carvedilol-treated (G), propranolol-treated (H), prazosin-treated (I), and atropine-treated (J) groups. All scale bars: 20 μm. Data are presented as mean ± SEM, with data points of individual animals. n denotes number of animals used for each group. * p < 0.05, ** p < 0.01, *** p < 0.001; n.s., not significant; two-tailed t test.

See also Figure S1.

zebrafish orthologs of these receptors, *adra1aa*, *adra1ab*, *adra1ba*, *adra1bb*, and *adra1d*, only *adra1d* and *adra1bb* showed considerable expression in the regenerating zebrafish heart, according to the searchable databases http://zebrafish.genomes.nl/tomoseq/ and http://www.zfregeneration.org/.[50,51] *adra1d* was transiently upregulated during the initial pro-inflammatory stage, but rapidly suppressed by 3 dpi, while *adra1bb* expression appeared to be induced consecutively and continued toward later stages of cardiac repair. On the basis of this expression analysis, we decided to focus our attention on the role of *adra1bb* in cardiac repair. adr1bb expression in macrophages, isolated from zebrafish larvae by fluorescence-acti-

vated cell sorting (FACS), was confirmed by quantitative reverse transcriptase PCR (qRT-PCR) (Figure S1D). To interfere with the signaling downstream of Adra1bb specifically in macrophages, we expressed the gene encoding Adra1bb third intracellular loop (hereinafter referred to as *adra1-3i*) in macrophages using the newly generated transgenic line *UAS:adra1-3i-T2A-CFP*, in combination with the macrophage-specific Gal4-driver line *csf1ra:Gal4* (Figure 2A). The *csf1ra:Gal4; UAS:adra1-3i-T2A-CFP; UAS:NTR-mCherry* line exhibited mosaic expression of *adra1-3i* in approximately 45% of all macrophages (labeled by NTR-mCherry) (Figures S2A–S2D). The mosaicism, possibly enhanced by competitiveness of the dual UAS system
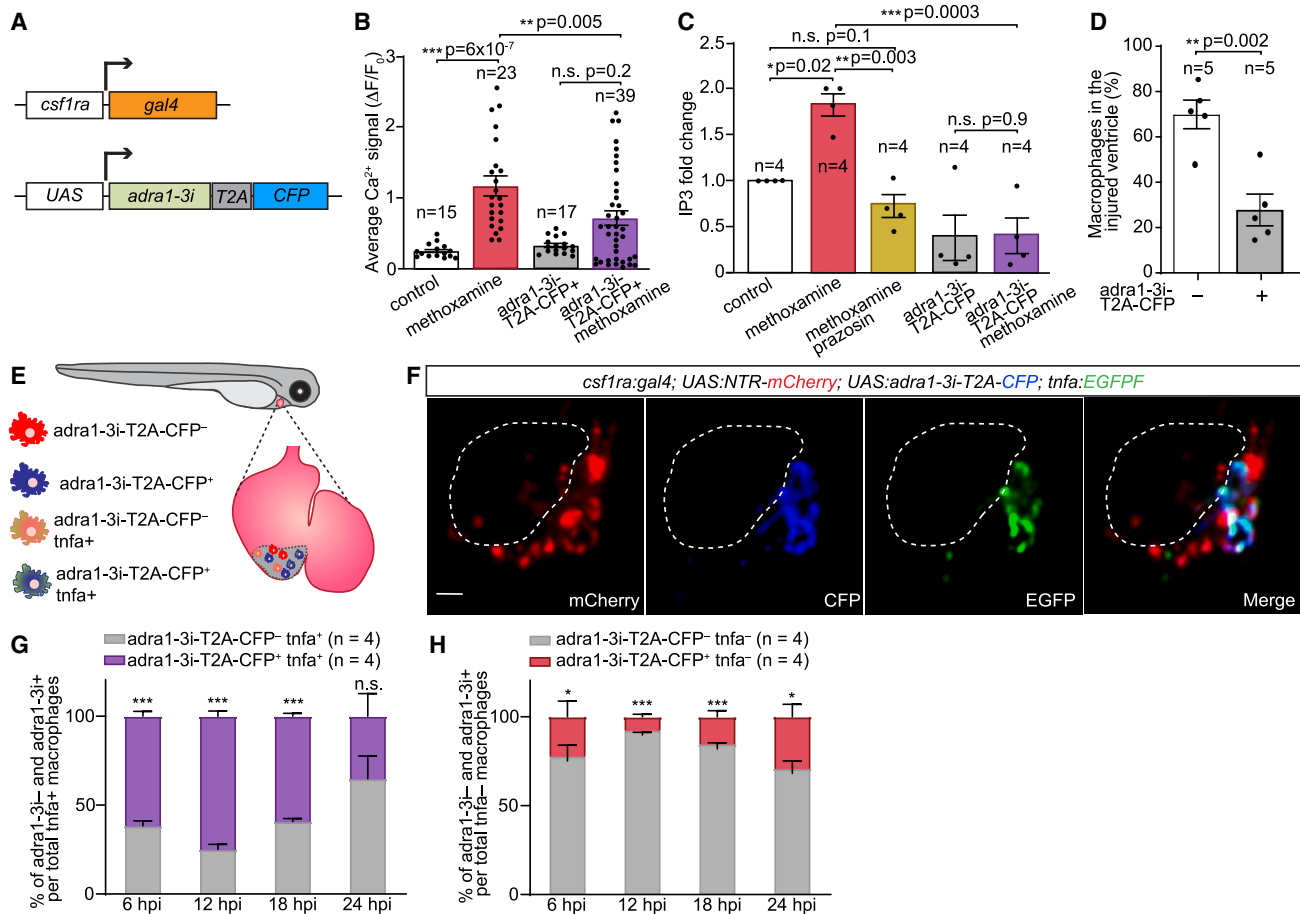
Figure 2. Non-inflammatory polarization of macrophages requires cell-autonomous adrenergic receptor alpha 1 (Adra1) signaling

(A) Scheme of the *UAS:adra1-3i-T2A-CFP* transgenic construct, used in combination with the *csf1ra:Gal4* line to drive its macrophage-specific expression.

(B and C) Bar graphs showing Adra1-3i-mediated impairment of calcium signaling (B) and inositol trisphosphate (IP3) production (C) in 5 dpf larvae following application of the Adra1 agonist methoxamine and/or its antagonist prazosin. Calcium signals were measured by time-lapse imaging of control *adra1-3i-T2A-CFP$^-$* and *adra1-3i-T2A-CFP$^+$* macrophages present in the same *csf1ra:Gal4; UAS:NTR-mCherry; UAS:adra1-3i-T2A-CFP; 14XUAS:GCaMP6s* larvae and shown as change of fluorescent intensity (ΔF) relative to fluorescence in resting condition (F_0). IP3 amounts were measured by ELISA of control (*tbp:Gal4*) and *adra1-3i-T2A-CFP*-expressing (*tbp:Gal4; UAS:adra1-3i-T2A-CFP*) larvae, and presented as fold change relative to unstimulated controls.

(D) Bar graph depicting percentages of *adra1-3i$^-$* and *adra1-3i$^+$* macrophages recruited to the hearts of 7 dpf *csf1ra:Gal4; UAS:NTR-mCherry; UAS:adra1-3i-T2A-CFP* larvae 24 h after two-photon laser injury.

(E) Diagram illustrating heterogeneous macrophage pools in *csf1ra:Gal4; UAS:NTR-mCherry; UAS:adra1-3i-T2A-CFP; tnfa:EGFPF* larvae.

(F) A representative heart of a 7-dpf *csf1ra:Gal4; UAS:NTR-mCherry; UAS:adra1-3i-T2A-CFP; tnfa:EGFPF* larva showing all recruited macrophages (mCherry$^+$) and *adra1-3i$^+$* (CFP$^+$) and *tnfa$^+$* (EGFP$^+$) ones 24 hpi induced with a two-photon laser. Dashed lines mark injury site. Scale bar: 20 μm.

(G and H) Segmented bar graphs displaying distribution of *adra1-3i$^-$* and *adra1-3i$^+$* macrophages within the pro-inflammatory (*tnfa$^+$*) (G) and non-inflammatory (*tnfa$^-$*) (H) macrophage populations recruited to the *csf1ra:Gal4; UAS:NTR-mCherry; UAS:adra1-3i-T2A-CFP; tnfa:EGFPF* larval heart at 6–24 hpi. Data are presented as mean ± SEM, with data points of individual animals or independent experiments. n denotes number of cells from 12 to 15 larvae per treatment group (B), biological replicates (each was a pool of 30 larvae) (C), or animals (D, G, and H) per group. * $p < 0.05$, ** $p < 0.01$, *** $p < 0.001$; n.s., not significant, two-tailed t test.

See also Figure S2.

(Figures S2E–S2H), allows assessment of functional alterations of macrophages carrying the *adra1-3i* transgene as compared with control macrophages lacking *adra1-3i* expression present in the same animals. We first tested efficiency of the loss-of-function approach by assessment of two main outcomes of Adra1 receptor signal transduction, increases of intracellular Ca^{2+} and IP3 production. When stimulated with the α1-adrenergic agonist methoxamine, control macrophages (with no *adra1-3i* expression) responded by rapid elevation of intracellular Ca^{2+}, measured with the genetically encoded calcium

indicator GCaMP6s in 5 dpf *csf1ra:Gal4; UAS:NTR-mCherry; UAS:adra1-3i-T2A-CFP; 14XUAS:GCaMP6s* larvae (Figure 2B). Expression of *adra1-3i* effectively hindered this Ca^{2+} rise, as no significant change in intracellular Ca^{2+} concentration was observed in these cells upon methoxamine stimulation (Figure 2B). In 5 dpf *tbp:Gal4; UAS:adra1-3i-T2A-CFP* larvae expressing *adra1-3i* ubiquitously, methoxamine stimulation increased ELISA-measured IP3 level in control *tbp:Gal4* larvae, an effect that was abolished in the presence of the α1-blocker prazosin. Importantly, IP3 elevation was blocked in *adra1-3i*

larvae (Figure 2C). Together, these data demonstrate that *adra1-3i* is a viable, dominant negative loss-of-function tool that allows efficient cell-type-specific inhibition of intrinsic Adra1 downstream signaling. In line with our previous experiment with prazosin-mediated global inhibition of α1-adrenergic receptor activation, Adra1 signaling inhibition in macrophages impaired their response to laser-induced necrosis of the heart at 7 dpf, as evidenced from fewer *adra1-3i*$^+$ macrophages recruited to the heart at 24 h post injury (hpi), compared with control *adra1-3i*$^-$ cells in the same larvae (Figure 2D).

Following cardiac injury, macrophages display a biphasic response to coordinate wound healing in zebrafish, characterized by early recruitment of pro-inflammatory macrophages followed by their phenotypic conversion to suppress inflammation and stimulate tissue remodeling.[52] *tnfa* expression level distinguishes these phenotypically and functionally diverse macrophage pools. Elevated expression of *tnfa* marks classically activated (M1)-like macrophages, whereas the *tnfa*$^-$ population exhibits alternatively activated (M2) macrophage phenotypes.[52] We used *csf1a:Gal4; UAS:adra1-3i-T2A-CFP; UAS:NTR-mCherry; tnfa:EGFPF* fish (Figures 2E and 2F) to identify M1-like (*tnfa*$^+$) and M2-like (*tnfa*$^-$) macrophages at different time points after injury. Intriguingly, distinct macrophage subsets were differentially affected by Adra1 loss-of-function. Indeed, we found that the decrease of macrophage numbers in the heart following laser-induced necrosis, caused by *adra1-3i* expression (Figure 2D), was not due to a reduction in the *tnfa*$^+$ pool because the majority of *tnfa*$^+$ macrophages recruited to the injured heart were *adra1-3i*$^+$ (Figure 2G). Conversely, the majority of cells in the *tnfa*$^-$ macrophage pool were *adra1-3i*$^-$ throughout the observation time (Figure 2H). These findings, therefore, suggested that Adra1 signaling is required to promote the presence of non-inflammatory macrophages at the injury site.

Global or macrophage-specific inhibition of Adra1 signaling impairs non-inflammatory macrophage response and cardiomyocyte mitotic activity in cryoinjured adult zebrafish hearts

To confirm the requirement of Adra1 signaling for the regenerative ability of the myocardium, and to further characterize response to injury of different macrophage populations in a model that could recapitulate cellular events occurring in myocardial infarction, we assessed adult zebrafish hearts after cardiac cryoinjury. Adult *csf1ra:Gal4; UAS:NTR-mCherry* zebrafish treated with prazosin from 1 to 7 dpi displayed no significant increase in proliferating cardiomyocytes compared with vehicle-treated control hearts (Figures 3A and 3B). Sham-operated vehicle and prazosin treatment groups, used as additional controls for the experiment, showed comparably low mitotic activity, commonly observed in the quiescent adult myocardium (Figures 3A and 3B). Expansion of macrophages, detectable by mCherry immunostaining, was localized mainly within the lesion border zone of the damaged heart and was hindered by prazosin-mediated global inhibition of Adra1 signaling (Figures 3C and 3D). This effect was not due to impairment of macrophage proliferation, assessed by proliferating cell nuclear antigen (PCNA) immunofluorescence staining, which was robustly induced in both control and prazosin-treated cryoinjured hearts (Figures S3A and S3B).

Inhibition of Adra1 signaling in macrophages in the *csf1ra:Gal4; UAS:adra1-3i-T2A-CFP; UAS:NTR-mCherry* line similarly attenuated myocardial self-renewal, observed at 7 dpi (Figures 3E and 3F), compared with control *csf1ra:Gal4; UAS:NTR-mCherry* fish. Percentages of proliferating cardiomyocytes in *csf1ra:Gal4; UAS:adra1-3i-T2A-CFP; UAS:NTR-mCherry* hearts after injury were indeed comparable to sham operation, indicating the requirement of macrophage Adra1 signaling for myocardial regenerative response. In agreement with our data in larvae (Figures 1F, 1I, 2G, and 2H), lesion in *csf1ra:Gal4; UAS:adra1-3i-T2A-CFP; UAS:NTR-mCherry* adult hearts contained fewer macrophages (Figure S3C and S3D), with a higher abundance of *adra1-3i*$^+$ macrophages in the *tnfa*$^+$ pool (Figures 3G and 3H) and reduced contribution of the cells to the *tnfa*$^-$ pool (Figures 3G and 3I) compared with control *adra1-3i*$^-$ cells with normal Adra1 signaling. 7 dpi is a critical time point when initial inflammation subsides and collagen scar resolution commences, coinciding with the replacement of *tnfa*$^+$ macrophages with *tnfa*$^-$ ones in the lesioned zebrafish heart.[33] The fact that inhibition of Adra1 signaling shifts the balance of the macrophage pool toward the *tnfa*$^+$ population posits the requirement of cell-autonomous Adra1 signaling for phenotypic differentiation of the non-inflammatory macrophages. We next tested this hypothesis and further investigated its mechanistic underpinnings.

Adra1 signaling activates an "ECM remodeling" transcriptional program in a macrophage subset in the injured heart

Macrophages exist in diverse activation states, each of which might exert different functions in reparative and regenerative responses of the cardiac tissue. To better characterize macrophage diversity further from the *tnfa*$^+$/*tnfa*$^-$ dichotomous division, we next aimed to identify functional subsets affected by Adra1 signaling deficiency. Moreover, we wanted to gain insight into the molecular program underlying the Adra1-driven macrophage response. To this end, we carried out single-cell RNA sequencing (scRNA-seq) of cryoinjured *csf1ra:Gal4; UAS:adra1-3i-T2A-CFP; UAS:NTR-mCherry* hearts at 7 dpi. Exploiting the transgenic line, both *adra1-3i*$^+$ and control *adra1-3i*$^-$ macrophages from the same hearts could be sequenced together (Figure 4A), allowing us to reduce interindividual variability. Unbiased hierarchical clustering identified, among several cell types presented in the lesioned heart (Figure 4B), four transcriptionally defined macrophage clusters (Figures 4C–4E). The top 70 most differentially expressed genes in each cluster showed that cluster 1 highly expressed antigen-presenting and T cell-activating genes (such as *ctss2.1, ifi30, cd74a, cd74b, mhc2a,* and *mhc2dab*). Cluster 2 had a higher expression of genes involved in mitochondrial oxidative metabolism, a hallmark of M2 polarization,[53,54] in association with oxidative stress cytoprotection (such as *atp5mc1, atp5pd, cox6b1, cox6b2, cox7a2a,* and *pdrx6*). Cluster 3 was enriched in genes required for the acute phase of wound repair, including hemolytic-related antioxidation, platelet recruitment, and neutrophil chemotaxis (such as *hp, timp4.2, timp2b,* and *csf3b*). In addition, upregulation of glycolytic genes in this population (such as *aldocb* and *eno1a*) indicates that they have pro-inflammatory M1-like metabolism.[55–57] Cluster 4 expressed regulators of ECM remodeling and fibrosis (such as *mmp2, col1a1a, col1a2, col5a1, fn1b, sparc, mdka,* and *tagln*) (Figures 4D and 4E).
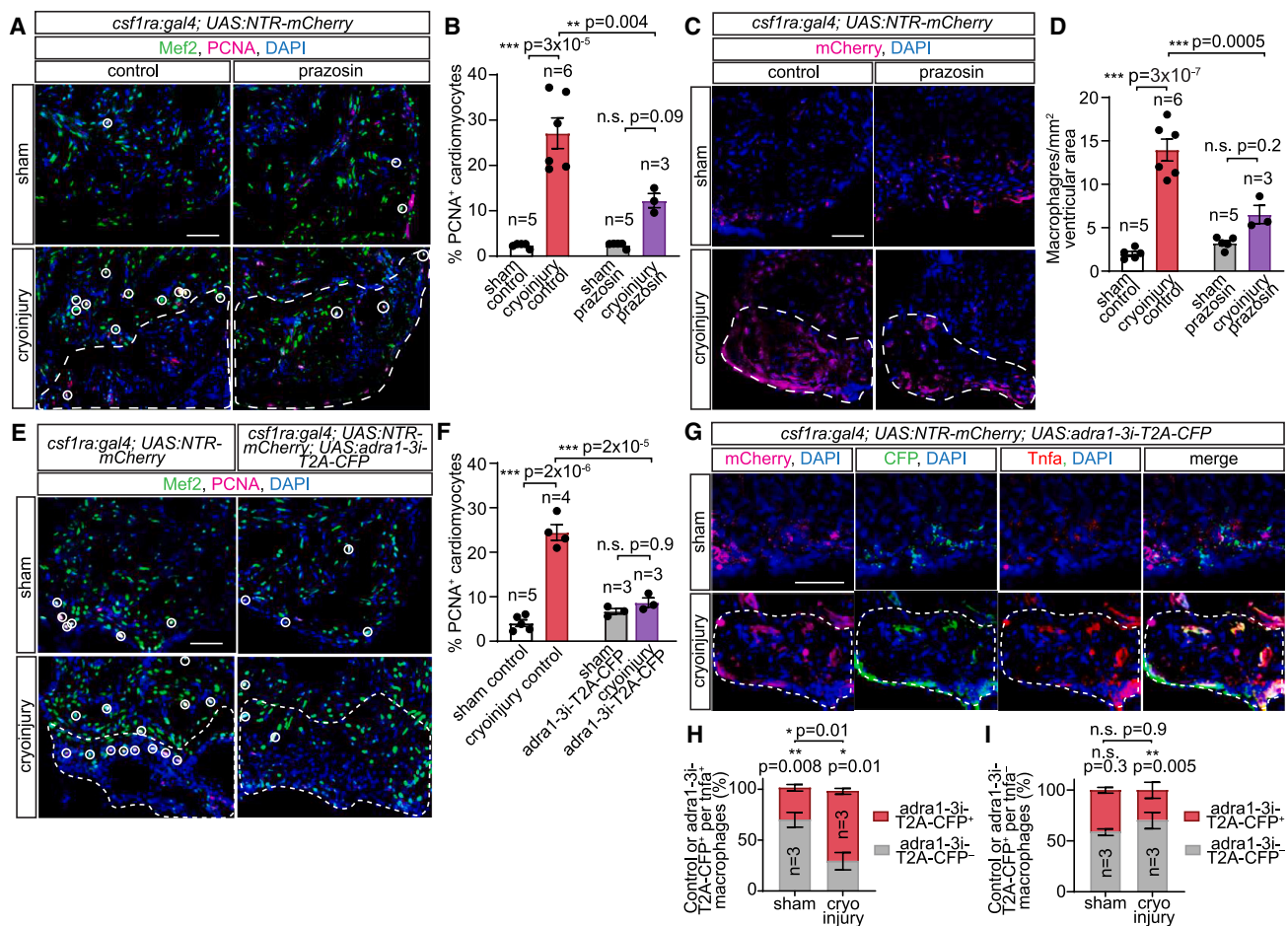
Figure 3. Adra1 signaling regulates macrophage phenotypes and cardiomyocyte proliferation during inflammatory/scar resolution in injured hearts

(A and B) Adult *csf1ra:Gal4; UAS:NTR-mCherry* hearts following sham operation or cryoinjury with control solution or prazosin treatment for 7 days. Immunofluorescent staining of Mef2 and PCNA labels cardiomyocytes and proliferating cells, respectively, in the heart cryosections (A). Proliferating cardiomyocytes (Mef2+/PCNA+) in the proximity of injury border zones, indicated by white circles (A) and quantified as percentages of cardiomyocytes within the observed area (B).

(C and D) Macrophages, labeled by mCherry immunostaining, in cryosections of hearts of adult *csf1ra:Gal4; UAS:NTR-mCherry* fish subjected to sham operation or cryoinjury, treated with control solution or prazosin for 7 days (C), and quantified as cell numbers per 1 mm² ventricular area (D).

(E and F) Proliferating cardiomyocytes in adult *csf1ra:Gal4; UAS:NTR-mCherry* (control) and *csf1ra:Gal4; UAS:NTR-mCherry; UAS:adra1-3i-T2A-CFP* (adra1-3i-T2A-CFP) animals labeled by immunofluorescent staining for Mef2 and PCNA, indicated by white circles (E) and quantified as percentages of PCNA+ cardiomyocytes within the observed area (F).

(G) Sham and cryoinjured *csf1ra:Gal4; UAS:NTR-mCherry; UAS:adra1-3i-T2A-CFP* heart sections, immunostained for mCherry (all macrophages), CFP (*adra1-3i-T2A-CFP+* macrophages), and Tnfa at 7 dpi.

(H and I) Segmented bar graphs showing distribution of *adra1-3i-T2A-CFP−* (control) and *adra1-3i-T2A-CFP+* macrophages within the pro-inflammatory (*tnfa+*) (H) and non-inflammatory (*tnfa−*) (I) pools present in sham-operated and cryoinjured hearts at 7 dpi. DAPI staining labeled all nuclei. Lesioned areas are outlined by white dashed lines. All scale bars: 50 μm. Data are presented as mean ± SEM, with data points of individual animals. n denotes number of animals measured in each group. * p < 0.05, ** p < 0.01, *** p < 0.001; n.s. not significant, two-tailed t test.

See also Figure S3.

Strikingly, while different functional subsets of *adra1-3i+* macrophages were similarly distinguished by these cluster-defining genes, as in control macrophages (Figures 4D and 4E), the macrophage pool in which Adra1 signaling was inhibited did not contain cluster 4 cells (Figures 4C and 4D), indicating that neurotransmitter receptor signaling is a prerequisite for activation of this ECM remodeling transcriptional program. Similar cellular compositions and the four macrophage subpopulations identifiable by the same gene sets were also present in cryoinjured con-

trol *csf1ra:Gal4; UAS:NTR-mCherry* fish in which Adra1 signaling is not inhibited (Figures S4A–S4D). Enrichment of *adra1bb* expression, with negligible level of *adra1d*, was apparent in cluster 4 macrophages (Figures S4E and S4F), further supporting a specialized role of the macrophage cell-autonomous adrenergic signaling, mediated by Adra1bb, primarily in the acquisition of the cluster 4 identity. Expression of prime fibrotic genes, including *cola1a*, *fn1b*, and *tagln* in a subset of macrophages, detectable by the presence of mCherry, was also validated by hybridization
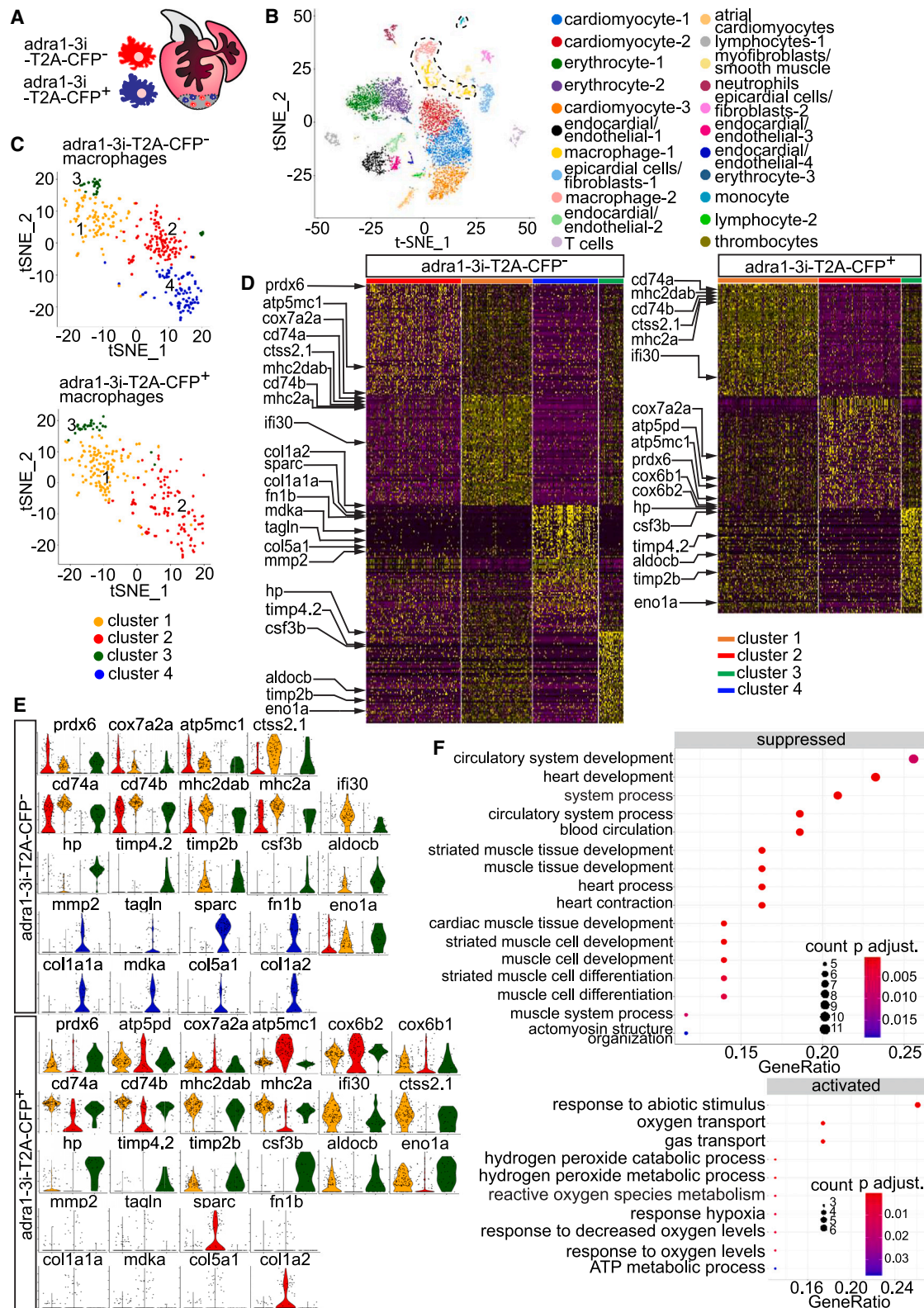
Figure 4. Adra1 activates an "extracellular matrix (ECM) remodeling" transcriptional program in a macrophage subset

(A) Diagram showing mixed populations of control (*adra1-3i-T2A-CFP⁻*) and Adra1-signaling-deficient (*adra1-3i-T2A-CFP⁺*) macrophages present in the same cryoinjured heart.

(legend continued on next page)

chain reaction (HCR)-fluorescence *in situ* hybridization (FISH), and immunofluorescence of *csf1ra:Gal4; UAS:NTR-mCherry* and *csf1ra:Gal4; UAS:adra1-3i-T2A-CFP; UAS:NTR-mCherry* hearts at 7 dpi (Figure S4G). Moreover, in support of the Adra1 signaling requirement for activation of cluster 4 macrophages, cryoinjured *csf1ra:Gal4; UAS:adra1-3i-T2A-CFP; UAS:NTR-mCherry* hearts contained fewer fn1b+/col1a1a+ macrophages (Figure S4H) and lower percentages of macrophages located within the proximity of the lesion turning on expression of these genes (Figure S4I). Interestingly, pathway analysis comparing *adra1-3i+* to control *adra1-3i-* macrophages showed suppression of heart/muscle cell/circulatory system developmental pathways (Figure 4F), highlighting the involvement of Adra1-activated macrophages in a tissue regenerative program, commonly involved in the rejuvenation of matured cells toward a developmental-like state.[58] Upregulation of hydrogen peroxide/reactive oxygen species metabolic processes in the *adra1-3i+* macrophage population, in line with our observation of their skewed distribution toward *tnfa+* pool, implicates the dispensability of Adra1 in the pro-inflammatory activation of macrophages.

Collectively, our findings identify the role of Adra1 signaling to determine subtype-specific activation of macrophages during the transition from acute inflammation to initiation of the fibrotic resolution phase of the cardiac regenerative program. The transcriptomic profile of the macrophage population implicates the macrophage subset in remodeling of the wound through ECM modification, a critical process in fibrotic regulation and replacement of the fibrous scar with new cardiac tissue.

Adra1-activated macrophages mediate collagenous scar turnover, fibroblast activation, and blood and lymphatic vessel regrowth during cardiac regeneration

To assess the effect of impaired activation of the ECM remodeling macrophage subset as a result of Adra1-signaling inhibition in scar modification, we first examined acid fuchsin orange-G (AFOG) staining of *csf1ra:Gal4; UAS:adra1-3i-T2A-CFP; UAS:NTR-mCherry* and control *csf1ra:Gal4; UAS:NTR-mCherry* sham-operated or cryoinjured hearts at 7 dpi. Deposition of fibrin- and collagen-rich ECM in lesioned areas was noticeably reduced upon blockage of macrophage Adra1 activation (Figures 5A and 5B). Accordingly, immunofluorescence staining showed that injury-induced production of type-1 collagen fibrils, the major structural component of the fibrotic ECM, was blunted in the *csf1ra:Gal4; UAS:adra1-3i-T2A-CFP; UAS:NTR-mCherry* hearts (Figures 5C and 5D). Moreover, staining of the hearts with collagen hybridizing peptide (CHP), which binds with very high specificity to unfolded collagen following degradation by collagenolytic proteases,[59] showed lower levels of degraded

collagen in cryoinjured *csf1ra:Gal4; UAS:adra1-3i-T2A-CFP; UAS:NTR-mCherry* hearts compared with controls (Figures 5E and 5F). These results, together with our scRNA-seq data showing absence of ECM remodeling characteristics among macrophages with impaired Adra1 signaling, unveil a critical role of the Adra1-activated macrophage subset in fibrotic scar turnover through the contribution of ECM proteins and promotion of proteolysis of ECM components.

The primary cell type responsible for ECM deposition in the infarcted wound is the myofibroblast, converted mainly from the fibroblast upon injury.[60] In the regenerating zebrafish heart, activated fibroblasts, detectable by induction of periostin (*postnb*) expression, have been reported to upregulate several matrix metalloproteinases in addition to different collagen subtypes and fibronectin. Ablation of col1a1-producing cells, to which *postnb+*-activated fibroblasts partly contributed, impaired cardiomyocyte proliferation, indicating the proregenerative role of fibrotic cells.[15] Therefore, we next examined whether the reduction of collagen deposition and impairment of ECM turnover when macrophage Adra1 signaling was inhibited might be attributed to compromised profibrotic activation of fibroblasts. Our analyses showed that cryoinjury-induced activation of fibroblasts, detected by HCR-FISH of *postnb*, was unaltered by macrophage Adra1 loss-of-function in the heart of *csf1ra:Gal4; UAS:adra1-3i-T2A-CFP; UAS:NTR-mCherry* fish compared with control *csf1ra:Gal4; UAS:NTR-mCherry* hearts (Figures 5G and S5A). However, fewer profibrotic fibroblasts co-expressing *postnb*, alpha smooth muscle actin (α-Sma), and collagen 1 (Col1) were found within the lesion area of the *csf1ra:Gal4; UAS:adra1-3i-T2A-CFP; UAS:NTR-mCherry* hearts (Figures 5G and 5H), suggesting the involvement of Adra1-activated macrophages in fibroblast differentiation.

The dynamic change of ECM content serves central roles in cardiac regeneration that extend beyond regulation of tissue stiffness and scar resolution. Proteolytic digestion of ECM controls the availability of various growth factors that can determine the behavioral responses of different cell types crucial to generating a proregenerative cardiac microenvironment to aid myocardial regrowth.[61,62] Therefore, we next tested whether the ECM-modulated cellular processes, including angiogenesis, lymphangiogenesis, and reinnervation of myocardial lesion, are affected by Adra1 loss-of-function in macrophages. *csf1ra:Gal4; UAS:adra1-3i-T2A-CFP; UAS:NTR-mCherry* hearts exhibited stunted injury-induced blood and lymphatic vessel growth in comparison with control *csf1ra:Gal4; UAS:NTR-mCherry* hearts, measured from immunofluorescent-labeling of cluster of differentiation 31 (CD31) in vascular endothelial cells (Figures 5I and 5J) and HCR-FISH hyaluronan receptor 1 (*lyve1*) in lymphatic

(B) t-distributed stochastic neighbor embedding (t-SNE) representation of whole-heart single-cell clustering. Dashed line outlines all macrophage/monocyte populations. A pool of 3 hearts was analyzed.

(C) t-SNE dimensionality reduction representation of 4 clusters in the *adra1-3i-T2A-CFP-* and 3 clusters in *adra1-3i-T2A-CFP+* populations.

(D) Heatmap of the 70 most differentially expressed genes in each cluster from (C) showed comparable expression profiles of the shared clusters (clusters 1–3), and cluster-defining genes of cluster 4 (ECM remodeling), present only in the *adra1-3i-T2A-CFP-* macrophage pool.

(E) Violin plots of cluster-defining genes depicted in (D).

(F) Gene ontology (GO) enrichment of differentially up- (activated) and downregulated (suppressed) genes in the Adra1-signaling-deficient (*adra1-3i-T2A-CFP+*) versus control (*adra1-3i-T2A-CFP-*) macrophages, displayed as gene ratio (differentially expressed genes related to GO term/total number of differentially expressed genes). Dot size in the graph represents number of differentially expressed genes enriched in a GO term (count). Bonferroni-Holm adjusted p values are represented with color scale of the dots.
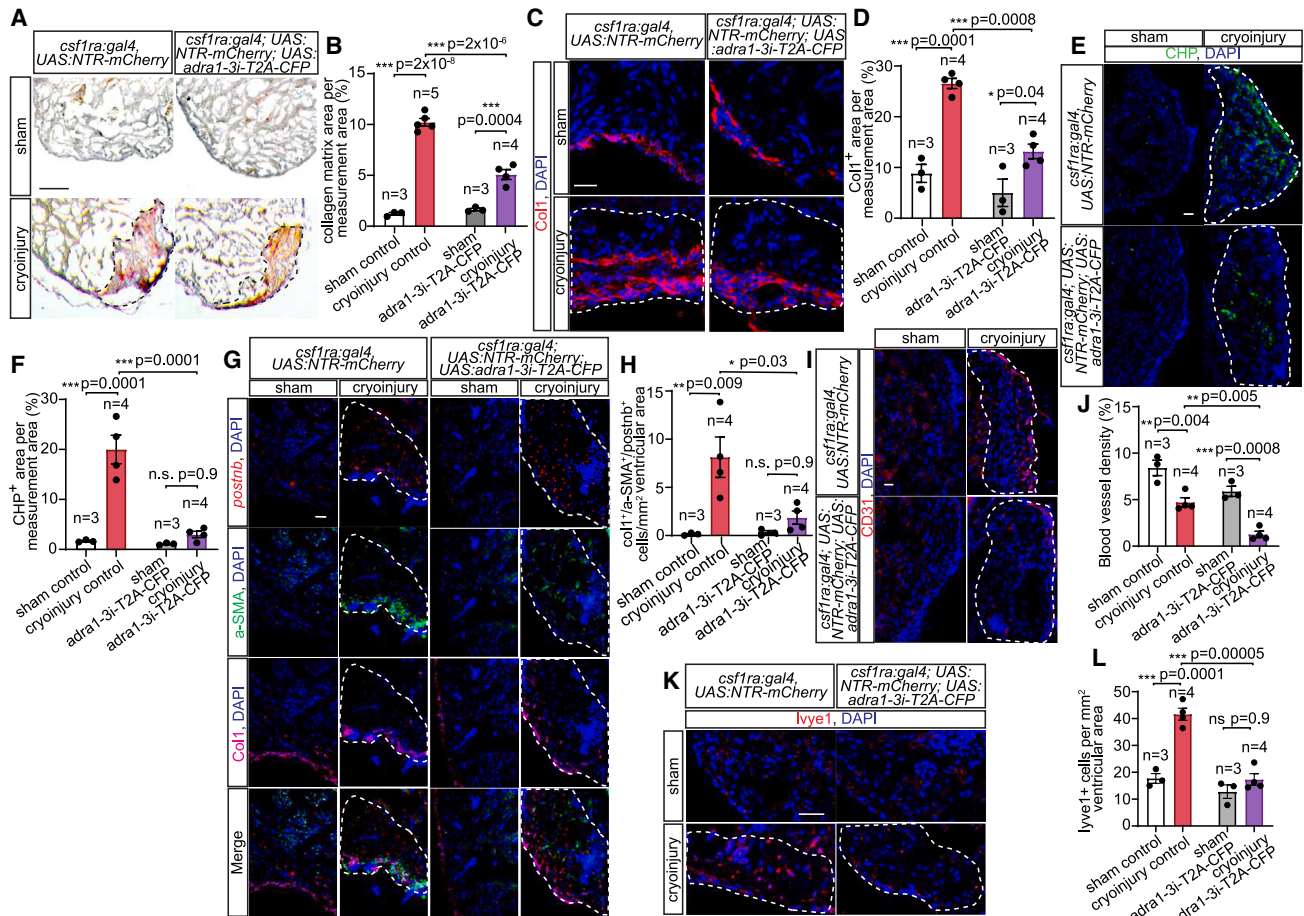
See also Figure S4.

Figure 5. Requirement of Adra1-activated macrophages for deposition and degradation of collagenous ECM, fibroblast activation, and re-vascularization of myocardial lesion

(A and B) Histological acid fuchsin orange-G (AFOG) staining of sham-operated or cryoinjured control and macrophage Adra1-signaling-deficient adult heart sections at 7 dpi (A), quantified as a percentage of area covered by collagen within the measurement area (B). Healthy muscles are stained in brown, fibrin in red, and collagen in blue.

(C and D) Collagen I (Col1) deposition in sham-operated and cryoinjured control and macrophage Adr1-signaling-deficient heart sections at 7 dpi, assessed by immunofluorescence (C) and measured as percentages of area of the ventricle (D).

(E and F) Degraded collagen in sham-operated and cryoinjured control and macrophage Adra1-signaling-deficient heart sections at 7 dpi, labeled by collagen hybridizing peptide (CHP) (E) and measured as percentages of area of the ventricle (F).

(G and H) Activated fibroblasts detected in heart sections from sham-operated and cryoinjured control and macrophage Adra1-signaling-deficient adult fish by HCR-FISH of activated fibroblast marker *periostin* (*postnb*), and immunofluorescent staining of profibrotic fibroblast marker alpha smooth muscle actin (α-SMA), and Col1 at 7 dpi (G), and quantified as col1$^+$a-SMA$^+$postnb$^+$ cells per 1 mm^2 area of the ventricle (H).

(I–L) Blood and lymphatic vasculatures in sham-operated and cryoinjured control and Adra1-signaling deficient heart sections were detected by immunofluorescence staining of CD31 (l) and HCR-FISH for *lyve1* (K) at 7 dpi and quantified as percentages of vessel area (J) or number of endothelial cells over total area measured (L). Scale bar: 0.1 mm (A) and 20 μm (C, E, G, I, and K). White dashed lines demarcate injured areas. Control: *csf1ra:Gal4; UAS:NTR-mCherry*. Macrophage Adra1-signaling-deficient (adra1-3i-T2A-CFP): *csf1ra:Gal4; UAS:NTR-mCherry; UAS:adra1-3i-T2A-CFP*. Data are presented as mean ± SEM, with data points of individual animals. n denotes number of animals included in each treatment group. * p < 0.05, ** p < 0.01, *** p < 0.001; n.s. not significant, two-tailed t test. See also Figure S5.

endothelial cells (Figures 5K and 5L). Innervation of the lesion, visualized by acetylated alpha-tubulin (acTub) immunofluorescence was unaffected (Figures S5B and S5C).

Midkine-mediated paracrine crosstalk between Adra1-activated macrophages and cardiac fibroblasts determines proregenerative fibroblast differentiation

Diverse populations of cardiac fibroblasts, originating from different cell types and existing in different activation states, are key players in transient fibrosis and the regenerative capability of the zebrafish heart.[63] Based on differential expression profiles reported previously,[63] distinct subsets of epicardial- and endocardial-derived fibroblasts were present in the *csf1ra:Gal4; UAS:adra1-3i-T2A-CFP; UAS:NTR-mCherry* hearts at 7 dpi (Figure 6A) and the control *csf1ra:Gal4; UAS:NTR-mCherry* hearts (Figures S6A and S6B). Distinct expression of several matrix proteins and proteolytic enzymes that are hallmarks of the previously defined proregenerative *col12a1a*$^+$ fibroblast subset, depletion of
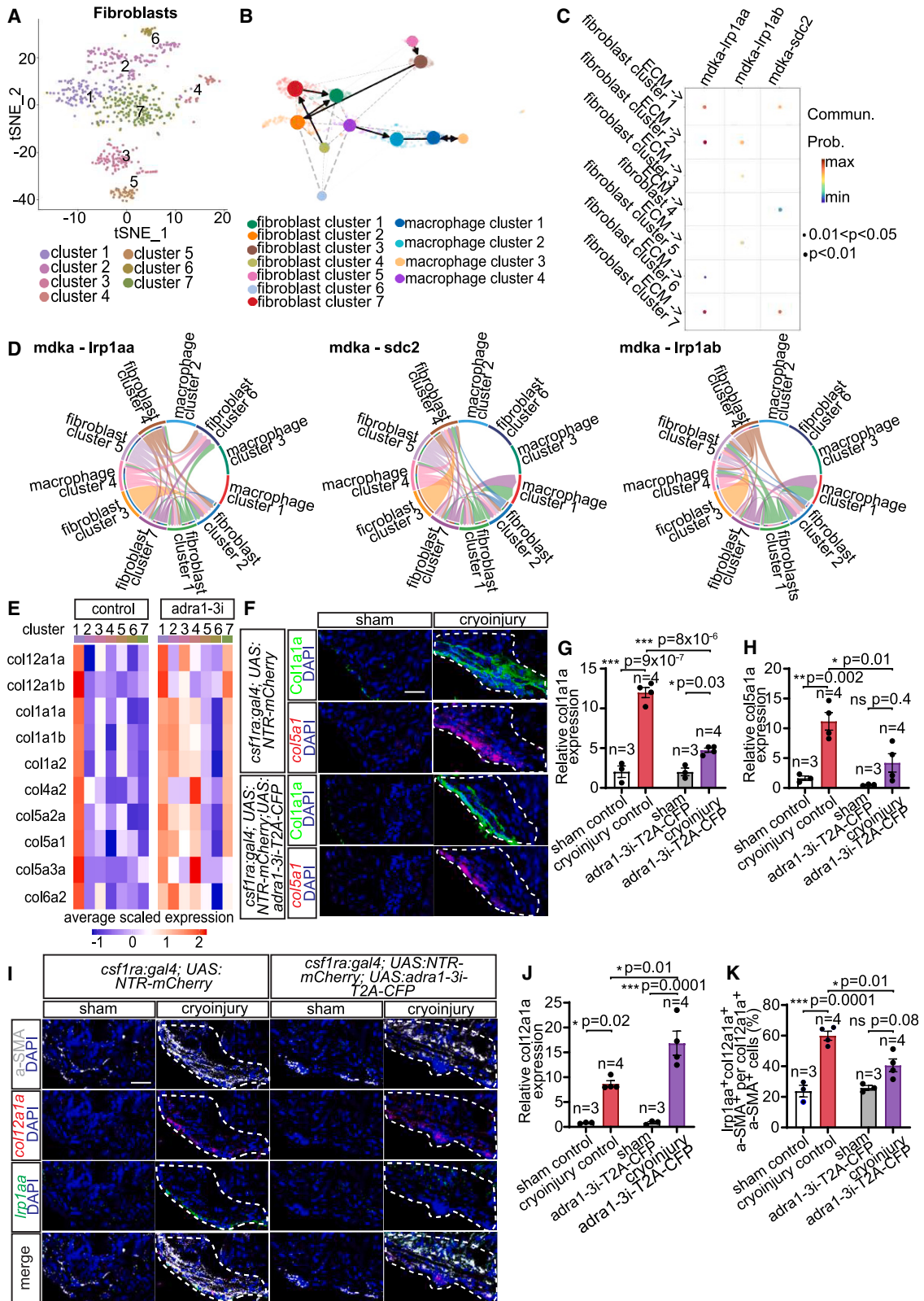
which impeded lesion healing and reduced cardiomyocyte proliferation,[63] led us to speculate that Adra1-activated ECM remodeling macrophages may contribute to this transiently activated fibroblast subset by transdifferentiation. However, integrated RNA velocity (Figure S6C) and single-cell trajectory inference (Figure 6B) showed no lineage relationship between macrophages and fibroblasts. In line with an earlier study,[63] *col12a1a*+ fibroblasts (cluster 1) observed in the *csf1ra:Gal4; UAS:adra1-3i-T2A-CFP; UAS:NTR-mCherry* hearts at 7 dpi were predicted to derive almost exclusively from fibroblasts cluster 7 (Figure 6B). Unlike cluster 1, cluster 7 cells showed low expression of profibrotic signatures, including *postnb*, *sparc*, *rgcc*, and *edil3a*, supporting the "pre-activated" state of the subset (Figure S6B). Next, to understand whether paracrine crosstalk underlies the influence of ECM remodeling macrophages on fibroblast activation and to identify potential signaling factors, we applied CellChat, a quantitative inference method for cell-cell communications based on expression of receptors, ligands, and other signaling cofactors,[64] to the *csf1ra:Gal4; UAS:adra1-3i-T2A-CFP; UAS:NTR-mCherry* whole-heart scRNA-seq dataset. CellChat identified fibroblast cluster 7 as a dominant communication partner with the highest sum of communication probabilities for outgoing signals from the ECM remodeling macrophage subset (Figures 6C and 6D). Macrophage-derived midkine a (Mdka), a pleiotropic heparin-binding peptide, and its receptors, including low-density lipoprotein-receptor-related protein 1Aa (Lrp1aa) and, with lower probability, the paralog lrp1ab and syndecan 2 (Sdc2), expressed in different fibroblast subsets, were predicted to mediate key signaling events (Figure 6C).

Our analyses hitherto suggested an Mdka-mediated signaling crosstalk between Adra1-activated macrophages and a specific fibroblast subset that serves as the precursor of *col12a1a*+ fibroblasts. To further test whether activation of *col12a1a*+ fibroblasts requires signaling input from the macrophage population, we compared expression profiles among fibroblast subclusters between 7 dpi control *csf1ra:Gal4; UAS:NTR-mCherry* and *csf1ra:Gal4; UAS:adra1-3i-T2A-CFP; UAS:NTR-mCherry* hearts. Unlike most other clusters in the *csf1ra:Gal4; UAS:adra1-3i-T2A-CFP; UAS:NTR-mCherry* heart, which appear to be akin to those identified in control hearts, cluster 7 and its descendant cells in cluster 1 displayed marked alteration of their expression profile

(Figure S6B). In particular, most collagens, both fibrillar and non-fibrillar subtypes (with the exception of *col12a1a*), which were expressed almost exclusively in *col12a1a*+ fibroblasts in control hearts, were not differentially expressed upon macrophage-specific Adra1 loss of function (Figure 6E). Aberrant expression of some of these genes, notably in fibroblast cluster 7, suggested an attempt at functional compensation (Figure 6E). To validate our findings from the computational approach, we assessed expression levels of different cluster-defining genes of *col12a1a*+ fibroblasts by HCR-FISH and immunofluorescence. As anticipated, expression of *col1a1a*, the predominant fibrillar component of the fibrotic tissue, was reduced in 7 dpi *csf1ra:Gal4; UAS:adra1-3i-T2A-CFP; UAS:NTR-mCherry* hearts (Figures 6F and 6G). Lower expression of *col5a1*, another fibrillar collagen reported to be a minor component of fibrotic tissue but serving a critical function to limit scar size after ischemic cardiac injury,[65] was also apparent upon macrophage Adra1-signaling deficiency (Figures 6F and 6H). Conversely, and in line with our scRNA-seq data, *csf1ra:Gal4; UAS:adra1-3i-T2A-CFP; UAS:NTR-mCherry* hearts showed higher expression of *col12a1a* (Figures 6I and 6J), the non-fibrillar collagen known to regulate collagen I fiber assembly and thereby promote tissue stiffness.[66] Finally, in contrast to control hearts in which Lrp1aa-activated cells constituted the majority of *col12a1a*+ fibroblasts at 7 dpi, the fibroblast subset detected in *csf1ra:Gal4; UAS:adra1-3i-T2A-CFP; UAS:NTR-mCherry* hearts failed to activate Lrp1aa in response to injury (Figures 6I and 6K).

To further validate Mdka as a signaling cue from Adra1-activated macrophages, we first examined whether Adra1 signaling deficiency alters *mdka* expression. Indeed, fewer *mdka*+ macrophages were observed at the lesioned sites of the *csf1ra:Gal4; UAS:adra1-3i-T2A-CFP; UAS:NTR-mCherry* as compared with control *csf1ra:Gal4; UAS:NTR-mCherry* hearts at 7 dpi (Figures 7A and 7B). Next, we proceeded to address the influence of Mdka antagonism on activation of the proregenerative *col12a1a*+ fibroblast subset and cardiac fibrosis in explanted zebrafish hearts following exposure to a recombinant zebrafish LDL-receptor-related protein associated protein 1 (Lrpap1) that we generated. LRPAP1, also known as RAP, is an endoplasmic reticulum protein that binds with high affinity to LRP1 and effectively prevents ligand association.[67] Treatment

Figure 6. Identification of fibroblast subpopulations and midkine (Mdka)-mediated paracrine crosstalk with Adra1-activated macrophages determining proregenerative matrix composition

(A) t-SNE representation of fibroblast clusters in 7 dpi *csf1ra:Gal4; UAS:NTR-mCherry; UAS:adra1-3i-T2A-CFP* hearts.

(B) Trajectory inference analysis suggested no lineage relationship between macrophages and fibroblasts, and fibroblast cluster 7 as a source of cluster 1 (*col12a1a*+ subset). The ECM remodeling population is macrophage cluster 4.

(C) Dot plot depicting significant ligand-receptor pairs inferred from CellChat contributing to signaling outputs from ECM remodeling macrophages to fibroblast populations. The dot color and size represent communication probability and p values, respectively.

(D) Chord diagram showing Mdka-mediated communications between all macrophage and fibroblast subsets. Colored segments indicate cell identity. Segment sizes depict interaction strength of the given receptor-ligand pair between the connected cell populations.

(E) Average expression of selected ECM components in fibroblast subclusters present in 7 dpi control and macrophage Adra1-signaling-deficient (adra1-3i) hearts.

(F–H) Expression of Col1a1a and *col5a1*, markers of *col12a1a*+ fibroblast subset, detected in heart sections by immunostaining and HCR-FISH, respectively (F), and quantified as integrated density of the signal normalized by measurement area (G and H).

(I–K) Expression of *col12a1a* and *lrp1aa* in the *col12a1a*+ fibroblast subset detected in 7 dpi *csf1ra:Gal4; UAS:NTR-mCherry* (control) and *csf1ra:Gal4; UAS:NTR-mCherry; UAS:adra1-3i-T2A-CFP* (adra1-3i-T2A-CFP) heart sections by immunofluorescence of a-SMA and HCR-FISH of *col12a1a* and *lrp1aa* (I). Bar graphs depicting integrated density of the *col12a1a* signal normalized by measurement area (J) and percentages of *lrp1aa*+*col12a1a*+a-SMA+ per total *col12a1a*+a-SMA+ fibroblasts (K). All scale bars: 20 μm. DAPI labeled all nuclei. White dashed lines demarcate injured areas. Data presented in bar graphs display mean ± SEM and data points of individual animals. n denotes number of animals measured for each group. * p < 0.05, ** p < 0.01, *** p < 0.001; n.s., not significant, two-tailed t test. See also Figure S6.
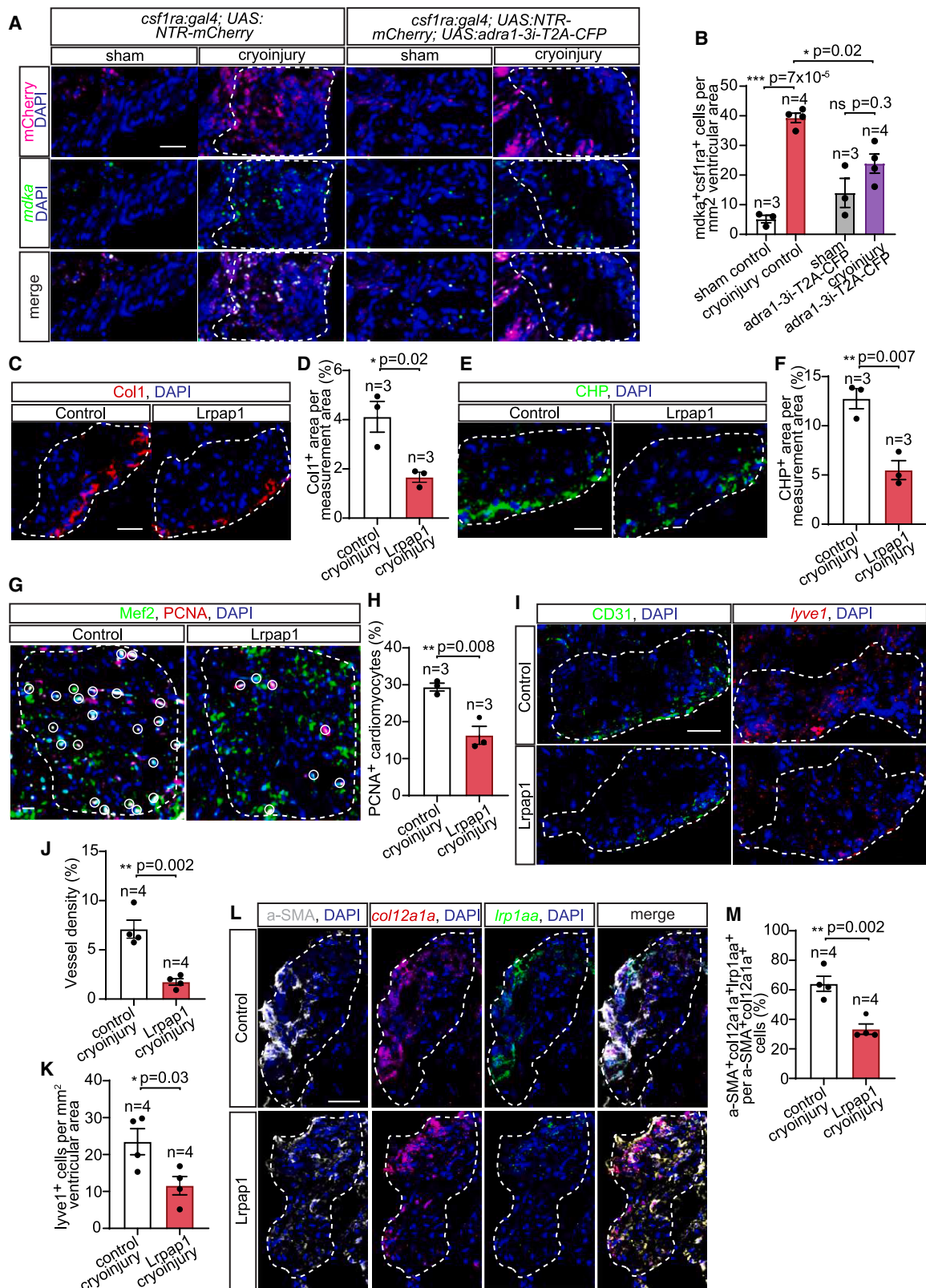
Figure 7. Mdka-Lrp1 signaling promotes *col12a1a*⁺ fibroblast activation, collagenous scar turnover, re-vascularization, and myocardial repair

(A and B) Macrophage (mCherry⁺) expression of *mdka*, detected by HCR-FISH, in sham-operated and cryoinjured *csf1ra:Gal4; UAS:NTR-mCherry* and *csf1ra:Gal4; UAS:NTR-mCherry; UAS:adra1-3i-T2A-CFP* heart section at 7 dpi (A), and quantified as numbers of mdka⁺mCherry⁺ cells per ventricular area (B).

(legend continued on next page)

with Lrpap1 impaired Col1 deposition and turnover assessed at 7 dpi in whole-heart explants (Figures 7C–7F). In line with dysregulated fibrosis, Lrpap1-treated explanted hearts were unable to induce cardiomyocyte proliferation or sprouting of the blood and lymphatic microvessels into the lesion (Figures 7G–7K). Lastly, decrease of *lrp1aa* fibroblasts in the *col12a1a*+ fibroblast subset (Figures 7L and 7M) further corroborated the role of Mdka-Lrp1aa signaling in macrophage-driven functional maturation of *col12a1a*+ fibroblasts.

Taken together, our data pinpoint a primary function of Adra1-acitvated macrophages in the establishment of a proregenerative cardiac microenvironment by determining the composition of a collagenous scar and its degradation dynamics, in part via paracrine activation of a proregenerative fibroblast subset, and promoting re-vascularization of the myocardial lesion.

DISCUSSION

We report here the role of neuro-immune crosstalk in the regulation of macrophage phenotypic reprogramming critical for mounting a myocardial regenerative response. Upon injury, macrophage cell-autonomous Adra1 signaling activates an ECM remodeling transcriptional program, characterized by the expression of different structural and matricellular components of cardiac ECM, and a proteolytic enzyme. Functionally, Adra1-activated macrophages engage intercellular Mdka-Lrp1aa signaling to activate a proregenerative fibroblast subset and determine composition of fibrillar and non-fibrillar collagens at the lesion site. The macrophage-fibroblast interplay identified here provides insight into the mechanism of fibrosis regulation and timely resolution critical to promote blood and lymphatic neovascularization and cardiomyocyte cell-cycle entry.

Impairment of Adra1 signaling in macrophages not only alters diversity of the innate cells but also the activation state of fibroblasts and ECM composition, all of which constitute the cellular and molecular makeups of the regenerative niche. Although commonly regarded as a flexible bridge of collagen I fibrils that can promote tissue regeneration,[68] wound repair is impeded by the aberrant production of collagen XII, which stalls pro-inflammatory macrophage at the wound bed.[69] Concomitantly, collagen V deficiency may further impair infarct healing by modulating the mechanical property of the scar, leading to dysregulated activation of fibroblasts.[65] Our identification of Mdka-Lrp1aa signaling crosstalk in macrophage-mediated activation of *col12a1a*+ fibroblasts, the major producer of these matrix components, suggests additional functions of the fibroblast subset in proregenerative niche remodeling. Lrp1 is an endocytic receptor that, in addition to mediating internalization of ECM proteins, cell-surface receptors, matrix metalloproteinase, and pro-

teinase inhibitors,[70] can also facilitate forward trafficking and assembly of co-receptors to initiate intracellular signaling.[71,72] Hence, Lrp1aa-expressing *col12a1a*+ fibroblasts may take part in the regulation of ECM remodeling, in part by balancing the availability of matrix modifying enzymes and their inhibitors within the fibrotic tissue.

It is commonly thought that pro-inflammatory monocytes infiltrating the infarcted heart early on switch their phenotype to give rise to the non-inflammatory macrophage pool critical to coordinate cardiac repair when initial inflammation subsides.[30,33] Another major macrophage pool is the cardiac-resident cells, colonizing the heart from early embryonic development prior to definitive hematopoiesis and maintained through local proliferation.[22] Resident macrophages in the neonatal mouse heart generate minimal inflammation and promote angiogenesis and cardiomyocyte proliferation.[21] In contrast, ischemic injury in adult mice markedly reduces the abundance of these cardioprotective resident cells.[25] To date, little is known about phenotypical and functional distinction between circulating monocytes and tissue-resident macrophages in zebrafish. The origin of Adra1-activated reparative macrophages as well as other phenotypically distinct subsets identified here is unclear. Reduction of macrophage numbers due to Adra1 loss-of-function during the inflammatory resolution/reparative phase of cardiac repair (24 hpi in larval and 7 dpi in adult hearts), despite the higher contribution of Adra1-signaling-deficient cells to the *tnfa*+ pro-inflammatory macrophages and normal proliferative rate, posits the possibility of Adra1-dependent extracardiac activation and recruitment of some of the reparative monocyte/macrophage populations. Concurrently, the fact that an aberrant proportion of the *tnfa*+ pool persisted in the lesioned hearts during this inflammatory and scar resolution phase upon Adra1 loss of function suggests that local Adra1 activation may participate in the phenotypic conversion of this macrophage pool at the injury site. Thus, Adra1 signaling activation of a reparative macrophage transcriptional program could take place in hematopoietic sites from which circulating monocytes egress or the cardiac tissue where resident cells are niched.

Limitations of the study

Cardiac tissue residency of the Adra1-activated macrophage population and location of the adrenergic input are yet to be defined. Determining the influence of microenvironmental cues to which these cells are exposed on the outcome of Adra1 activation will not only shed more light onto the mechanism of sympathetic control of macrophage response in cardiac regeneration but also aid the development of an effective strategy for regulation of fibrotic scarring and promoting regenerative repair post myocardial infarction. In addition, mechanistic

---

(C–F) Type-I collagen deposition (C) and collagen degradation (E) in control and Lrpap1-treated explanted heart sections, measured as percentages of Col1 (D) and CHP (F) area per injured ventricular area at 7 dpi.

(G and H) Proliferating cardiomyocytes (white circles), marked by immunofluorescent staining of 7 dpi control and Lrpap1-treated explanted heart sections with antibodies against PCNA and Mef2 (G), and measured as percentages of total cardiomyocytes within the measurement area (H).

(I–K) Blood and lymphatic vessel growth within the lesion of 7 dpi control and Lrpap1-treated heart explants detected by CD31 immunofluorescence and *lyve1* HCR-FISH, respectively (I), and measured as a percentage of vessel area (%) and number of endothelial cells over total area measured (J and K). *Lrp1aa*-expressing *col12a1a*+ fibroblast subset in control and Lrpap1-treated heart explants, marked by immunofluorescence of a-SMA and HCR-FISH of *col12a1a* and *lrp1aa* (L), and quantified as percentages of a-SMA+*col12a1a*+*lrp1aa*+ cells per total a-SMA+*col12a1a*+ fibroblasts (M). All scale bars: 20 μm. DAPI labeled all nuclei. White dashed lines demarcate injured areas. Data are displayed as mean ± SEM and data points of individual animals. n denotes number of animals measured for each group. * p < 0.05, ** p < 0.01, *** p < 0.001; n.s. not significant, two-tailed t test.

underpinning of Mdka-mediated proregenerative fibroblast activation requires further investigation.

STAR★METHODS

Detailed methods are provided in the online version of this paper and include the following:

- KEY RESOURCES TABLE
- RESOURCE AVAILABILITY
  - Lead contact
  - Materials availability
  - Data and code availability
- EXPERIMENTAL MODEL AND STUDY PARTICIPANT DETAILS
  - Animal care and strains
- METHOD DETAILS
  - Generation of expression constructs and transgenic animals
  - Imaging
  - Heart injury
  - Pharmacological treatments
  - Heart dissection and cryosectioning
  - Tissue dissociation
  - Production of recombinant Lrpap1
  - Explant culture and cryoinjury
  - ELISA
  - Calcium measurement
  - Immunofluorescence and histological staining
  - Acid Fuchsin Orange G (AFOG) staining
  - Hybridization chain reaction (HCR) and fluorescent in situ hybridization (FISH)
  - Image analyses
  - Fluorescent activated cell sorting (FACS)
  - Single cell RNA sequencing and analyses
- QUANTIFICATION AND STATISTICAL ANALYSIS

SUPPLEMENTAL INFORMATION

Supplemental information can be found online at https://doi.org/10.1016/j.devcel.2023.09.011.

AUTHOR CONTRIBUTIONS

Conceptualization, S.S.; methodology, O.A. and A.A.; investigation O.A. and A.A.; writing—original draft, O.A., A.F., and S.S.; writing—review and editing, O.A., A.F., and S.S.; funding acquisition, S.S.; project administration, S.S.; supervision, A.F. and S.S.

DECLARATION OF INTERESTS

The authors declare no competing interests.

REFERENCES

1. Nowbar, A.N., Gitto, M., Howard, J.P., Francis, D.P., and Al-Lamee, R. (2019). Mortality from ischemic heart disease. Circ. Cardiovasc. Qual. Outcomes 12, e005375. https://doi.org/10.1161/CIRCOUTCOMES.118.005375.

2. Roth, G.A., Mensah, G.A., Johnson, C.O., Addolorato, G., Ammirati, E., Baddour, L.M., Barengo, N.C., Beaton, A.Z., Benjamin, E.J., Benziger, C.P., et al. (2020). Global burden of cardiovascular diseases and risk factors, 1990–2019: update from the GBD 2019 study. J. Am. Coll. Cardiol. 76, 2982–3021. https://doi.org/10.1016/j.jacc.2020.11.010.

3. He, L., Nguyen, N.B., Ardehali, R., and Zhou, B. (2020). Heart regeneration by endogenous stem cells and cardiomyocyte proliferation: Controversy, Fallacy, and Progress. Circulation 142, 275–291. https://doi.org/10.1161/CIRCULATIONAHA.119.045566.

4. Kikuchi, K., and Poss, K.D. (2012). Cardiac regenerative capacity and mechanisms. Annu. Rev. Cell Dev. Biol. 28, 719–741. https://doi.org/10.1146/annurev-cellbio-101011-155739.

5. Bergmann, O., Bhardwaj, R.D., Bernard, S., Zdunek, S., Barnabé-Heider, F., Walsh, S., Zupicich, J., Alkass, K., Buchholz, B.A., Druid, H., et al. (2009). Evidence for cardiomyocyte renewal in humans. Science 324, 98–102. https://doi.org/10.1126/science.1164680.

6. Velagaleti, R.S., Pencina, M.J., Murabito, J.M., Wang, T.J., Parikh, N.I., D'Agostino, R.B., Levy, D., Kannel, W.B., and Vasan, R.S. (2008). Long-term trends in the incidence of heart failure after myocardial infarction. Circulation 118, 2057–2062. https://doi.org/10.1161/CIRCULATIONAHA.108.784215.

7. Cahill, T.J., Choudhury, R.P., and Riley, P.R. (2017). Heart regeneration and repair after myocardial infarction: translational opportunities for novel therapeutics. Nat. Rev. Drug Discov. 16, 699–717. https://doi.org/10.1038/nrd.2017.106.

8. Becker, R.O., Chapin, S., and Sherry, R. (1974). Regeneration of the ventricular myocardium in amphibians. Nature 248, 145–147. https://doi.org/10.1038/248145a0.

9. Flink, I.L. (2002). Cell cycle reentry of ventricular and atrial cardiomyocytes and cells within the epicardium following amputation of the ventricular apex in the axolotl, Amblystoma mexicanum: confocal microscopic immunofluorescent image analysis of bromodeoxyuridine-labeled nuclei. Anat. Embryol. (Berl) 205, 235–244. https://doi.org/10.1007/s00429-002-0249-6.

10. Poss, K.D., Wilson, L.G., and Keating, M.T. (2002). Heart regeneration in zebrafish. Science 298, 2188–2190. https://doi.org/10.1126/science.1077857.

11. Porrello, E.R., Mahmoud, A.I., Simpson, E., Hill, J.A., Richardson, J.A., Olson, E.N., and Sadek, H.A. (2011). Transient regenerative potential of the neonatal mouse heart. Science 331, 1078–1080. https://doi.org/10.1126/science.1200708.

12. Chablais, F., Veit, J., Rainer, G., and Jaźwińska, A. (2011). The zebrafish heart regenerates after cryoinjury-induced myocardial infarction. BMC Dev. Biol. 11, 21. https://doi.org/10.1186/1471-213X-11-21.

13. González-Rosa, J.M., Martín, V., Peralta, M., Torres, M., and Mercader, N. (2011). Extensive scar formation and regression during heart regeneration after cryoinjury in zebrafish. Development 138, 1663–1674. https://doi.org/10.1242/dev.060897.

14. Godwin, J.W., Debuque, R., Salimova, E., and Rosenthal, N.A. (2017). Heart regeneration in the salamander relies on macrophage-mediated control of fibroblast activation and the extracellular landscape. NPJ Regen. Med. 2, 1–11. https://doi.org/10.1038/s41536-017-0027-y.

15. Sánchez-Iranzo, H., Galardi-Castilla, M., Sanz-Morejón, A., González-Rosa, J.M., Costa, R., Ernst, A., Sainz de Aja, J.S., Langa, X., and

Mercader, N. (2018). Transient fibrosis resolves via fibroblast inactivation in the regenerating zebrafish heart. Proc. Natl. Acad. Sci. USA 115, 4188–4193. https://doi.org/10.1073/pnas.1716713115.

16. Sayers, J.R., and Riley, P.R. (2021). Heart regeneration: beyond new muscle and vessels. Cardiovasc. Res. 117, 727–742. https://doi.org/10.1093/cvr/cvaa320.

17. Steffens, S., Montecucco, F., and Mach, F. (2009). The inflammatory response as a target to reduce myocardial ischaemia and reperfusion injury. Thromb. Haemost. 102, 240–247. https://doi.org/10.1160/TH08-12-0837.

18. Formigli, L., Manneschi, L.I., Nediani, C., Marcelli, E., Fratini, G., Orlandini, S.Z., and Perna, A.M. (2001). Are macrophages involved in early myocardial reperfusion injury? Ann. Thorac. Surg. 71, 1596–1602. https://doi.org/10.1016/S0003-4975(01)02400-6.

19. Aurora, A.B., Porrello, E.R., Tan, W., Mahmoud, A.I., Hill, J.A., Bassel-Duby, R., Sadek, H.A., and Olson, E.N. (2014). Macrophages are required for neonatal heart regeneration. J. Clin. Invest. 124, 1382–1392. https://doi.org/10.1172/JCI72181.

20. Lai, S.L., Marín-Juez, R., Moura, P.L., Kuenne, C., Lai, J.K.H., Tsedeke, A.T., Guenther, S., Looso, M., and Stainier, D.Y.R. (2017). Reciprocal analyses in zebrafish and medaka reveal that harnessing the immune response promotes cardiac regeneration. eLife 6, 1–20. https://doi.org/10.7554/eLife.25605.

21. Lavine, K.J., Epelman, S., Uchida, K., Weber, K.J., Nichols, C.G., Schilling, J.D., Ornitz, D.M., Randolph, G.J., and Mann, D.L. (2014). Distinct macrophage lineages contribute to disparate patterns of cardiac recovery and remodeling in the neonatal and adult heart. Proc. Natl. Acad. Sci. USA 111, 16029–16034. https://doi.org/10.1073/pnas.1406508111.

22. Epelman, S., Lavine, K.J., Beaudin, A.E., Sojka, D.K., Carrero, J.A., Calderon, B., Brija, T., Gautier, E.L., Ivanov, S., Satpathy, A.T., et al. (2014). Embryonic and adult-derived resident cardiac macrophages are maintained through distinct mechanisms at steady state and during inflammation. Immunity 40, 91–104. https://doi.org/10.1016/j.immuni.2013.11.019.

23. Bajpai, G., Schneider, C., Wong, N., Bredemeyer, A., Hulsmans, M., Nahrendorf, M., Epelman, S., Kreisel, D., Liu, Y., Itoh, A., et al. (2018). The human heart contains distinct macrophage subsets with divergent origins and functions. Nat. Med. 24, 1234–1245. https://doi.org/10.1038/s41591-018-0059-x.

24. Bajpai, G., Bredemeyer, A., Li, W., Zaitsev, K., Koenig, A.L., Lokshina, I., Mohan, J., Ivey, B., Hsiao, H.M., Weinheimer, C., et al. (2019). Tissue resident CCR2- and CCR2+ cardiac macrophages differentially orchestrate monocyte recruitment and fate specification following myocardial injury. Circ. Res. 124, 263–278. https://doi.org/10.1161/CIRCRESAHA.118.314028.

25. Dick, S.A., Macklin, J.A., Nejat, S., Momen, A., Clemente-Casares, X., Althagafi, M.G., Chen, J., Kantores, C., Hosseinzadeh, S., Aronoff, L., et al. (2019). Self-renewing resident cardiac macrophages limit adverse remodeling following myocardial infarction. Nat. Immunol. 20, 29–39. https://doi.org/10.1038/s41590-018-0272-2.

26. Zaman, R., Hamidzada, H., and Epelman, S. (2021). Exploring cardiac macrophage heterogeneity in the healthy and diseased myocardium. Curr. Opin. Immunol. 68, 54–63. https://doi.org/10.1016/j.coi.2020.09.005.

27. Peet, C., Ivetic, A., Bromage, D.I., and Shah, A.M. (2020). Cardiac monocytes and macrophages after myocardial infarction. Cardiovasc. Res. 116, 1101–1112. https://doi.org/10.1093/CVR/CVZ336.

28. Mentkowski, K.I., Euscher, L.M., Patel, A., Alevriadou, B.R., and Lang, J.K. (2020). Monocyte recruitment and fate specification after myocardial infarction. Am. J. Physiol. Cell Physiol. 319, C797–C806. https://doi.org/10.1152/AJPCELL.00330.2020.

29. Nahrendorf, M., Swirski, F.K., Aikawa, E., Stangenberg, L., Wurdinger, T., Figueiredo, J.L., Libby, P., Weissleder, R., and Pittet, M.J. (2007). The healing myocardium sequentially mobilizes two monocyte subsets with divergent and complementary functions. J. Exp. Med. 204, 3037–3047. https://doi.org/10.1084/jem.20070885.

30. Hilgendorf, I., Gerhardt, L.M.S., Tan, T.C., Winter, C., Holderried, T.A.W., Chousterman, B.G., Iwamoto, Y., Liao, R., Zirlik, A., Scherer-Crosbie, M., et al. (2014). Ly-6 chigh monocytes depend on nr4a1 to balance both inflammatory and reparative phases in the infarcted myocardium. Circ. Res. 114, 1611–1622. https://doi.org/10.1161/CIRCRESAHA.114.303204.

31. Li, W., Hsiao, H.-M., Higashikubo, R., Saunders, B.T., Bharat, A., Goldstein, D.R., Krupnick, A.S., Gelman, A.E., Lavine, K.J., and Kreisel, D. (2016). Heart-resident CCR2+ macrophages promote neutrophil extravasation through TLR9/MyD88/CXCL5 signaling. JCI Insight 1, 87315. https://doi.org/10.1172/jci.insight.87315.

32. Sanz-Morejón, A., García-Redondo, A.B., Reuter, H., Marques, I.J., Bates, T., Galardi-Castilla, M., Große, A., Manig, S., Langa, X., Ernst, A., et al. (2019). Wilms tumor 1b Expression Defines a Pro-regenerative Macrophage Subtype and Is Required for Organ Regeneration in the zebrafish. Cell Rep. 28, 1296–1306.e6. https://doi.org/10.1016/j.celrep.2019.06.091.

33. Bevan, L., Lim, Z.W., Venkatesh, B., Riley, P.R., Martin, P., and Richardson, R.J. (2020). Specific macrophage populations promote both cardiac scar deposition and subsequent resolution in adult zebrafish. Cardiovasc. Res. 116, 1357–1371. https://doi.org/10.1093/CVR/CVZ221.

34. Simões, F.C., Cahill, T.J., Kenyon, A., Gavriouchkina, D., Vieira, J.M., Sun, X., Pezzolla, D., Ravaud, C., Masmanian, E., Weinberger, M., et al. (2020). Macrophages directly contribute collagen to scar formation during zebrafish heart regeneration and mouse heart repair. Nat. Commun. 11, 600. https://doi.org/10.1038/s41467-019-14263-2.

35. Lucas, T., Waisman, A., Ranjan, R., Roes, J., Krieg, T., Müller, W., Roers, A., and Eming, S.A. (2010). Differential roles of macrophages in diverse phases of skin repair. J. Immunol. 184, 3964–3977. https://doi.org/10.4049/jimmunol.0903356.

36. Pakshir, P., and Hinz, B. (2018). The big five in fibrosis: macrophages, myofibroblasts, matrix, mechanics, and miscommunication. Matrix Biol. 68–69, 81–93. https://doi.org/10.1016/j.matbio.2018.01.019.

37. Olofsson, P.S., Rosas-Ballina, M., Levine, Y.A., and Tracey, K.J. (2012). Rethinking inflammation: neural circuits in the regulation of immunity. Immunol. Rev. 248, 188–204. https://doi.org/10.1111/j.1600-065X.2012.01138.x.

38. Chavan, S.S., Pavlov, V.A., and Tracey, K.J. (2017). Mechanisms and therapeutic relevance of neuro-immune communication. Immunity 46, 927–942. https://doi.org/10.1016/j.immuni.2017.06.008.

39. Pavlov, V.A., Chavan, S.S., and Tracey, K.J. (2018). Molecular and functional neuroscience in immunity. Annu. Rev. Immunol. 36, 783–812. https://doi.org/10.1146/annurev-immunol-042617-053158.

40. Andersson, U., and Tracey, K.J. (2012). Reflex principles of immunological homeostasis. Annu. Rev. Immunol. 30, 313–335. https://doi.org/10.1146/annurev-immunol-020711-075015.

41. Tracey, K.J. (2002). The inflammatory reflex. Nature 420, 853–859. https://doi.org/10.1038/nature01321.

42. Olofsson, P.S., Katz, D.A., Rosas-Ballina, M., Levine, Y.A., Ochani, M., Valdés-Ferrer, S.I., Pavlov, V.A., Tracey, K.J., and Chavan, S.S. (2012). α7 nicotinic acetylcholine receptor (α7nAChR) expression in bone marrow-derived non-T cells is required for the inflammatory reflex. Mol. Med. 18, 539–543. https://doi.org/10.2119/molmed.2011.00405.

43. White, I.A., Gordon, J., Balkan, W., and Hare, J.M. (2015). Sympathetic reinnervation is required for mammalian cardiac regeneration. Circ. Res. 117, 990–994. https://doi.org/10.1161/CIRCRESAHA.115.307465.

44. Mahmoud, A.I., O'Meara, C.C., Gemberling, M., Zhao, L., Bryant, D.M., Zheng, R., Gannon, J.B., Cai, L., Choi, W.Y., Egnaczyk, G.F., et al. (2015). Nerves regulate cardiomyocyte proliferation and heart regeneration. Dev. Cell 34, 387–399. https://doi.org/10.1016/j.devcel.2015.06.017.

45. Woodcock, E.A., Du, X.-J., Reichelt, M.E., and Graham, R.M. (2008). Cardiac alpha 1-adrenergic drive in pathological remodelling. Cardiovasc. Res. 77, 452–462. https://doi.org/10.1093/cvr/cvm078.

46. Luttrell, L.M., Ostrowski, J., Cotecchia, S., Kendall, H., and Lefkowitz, R.J. (1993). Antagonism of catecholamine receptor signaling by expression of cytoplasmic domains of the receptors. Science 259, 1453–1457. https://doi.org/10.1126/science.8383880.

47. Kjelsberg, M.A., Cotecchia, S., Ostrowski, J., Caron, M.G., and Lefkowitz, R.J. (1992). Constitutive activation of the alpha 1B-adrenergic receptor by all amino acid substitutions at a single site. Evidence for a region which constrains receptor activation. J. Biol. Chem. 267, 1430–1433. https://doi.org/10.1016/S0021-9258(18)45962-5.

48. Scheer, A., Fanelli, F., Costa, T., De Benedetti, P.G., and Cotecchia, S. (1996). Constitutively active mutants of the α(1B)-adrenergic receptor: role of highly conserved polar amino acids in receptor activation. EMBO J. 15, 3566–3578. https://doi.org/10.1002/j.1460-2075.1996.tb00726.x.

49. Ahles, A., and Engelhardt, S. (2014). Polymorphic variants of adrenoceptors: pharmacology, physiology, and role in disease. Pharmacol. Rev. 66, 598–637. https://doi.org/10.1124/pr.113.008219.

50. Wu, C.C., Kruse, F., Vasudevarao, M.D., Junker, J.P., Zebrowski, D.C., Fischer, K., Noël, E.S., Grün, D., Berezikov, E., Engel, F.B., et al. (2016). Spatially resolved genome-wide transcriptional profiling identifies BMP signaling as essential regulator of zebrafish cardiomyocyte regeneration. Dev. Cell 36, 36–49. https://doi.org/10.1016/j.devcel.2015.12.010.

51. Nieto-Arellano, R., and Sánchez-Iranzo, H. (2019). ZfRegeneration: A database for gene expression profiling during regeneration. Bioinformatics 35, 703–705. https://doi.org/10.1093/bioinformatics/bty659.

52. Nguyen-Chi, M., Laplace-Builhe, B., Travnickova, J., Luz-Crawford, P., Tejedor, G., Phan, Q.T., Duroux-Richard, I., Levraud, J.P., Kissa, K., Lutfalla, G., et al. (2015). Identification of polarized macrophage subsets in zebrafish. eLife 4, e07288. https://doi.org/10.7554/eLife.07288.

53. Tan, Z., Xie, N., Cui, H., Moellering, D.R., Abraham, E., Thannickal, V.J., and Liu, G. (2015). Pyruvate dehydrogenase kinase 1 participates in macrophage polarization via regulating glucose metabolism. J. Immunol. 194, 6082–6089. https://doi.org/10.4049/jimmunol.1402469.

54. Mills, E.L., and O'Neill, L.A. (2016). Reprogramming mitochondrial metabolism in macrophages as an anti-inflammatory signal. Eur. J. Immunol. 46, 13–21. https://doi.org/10.1002/eji.201445427.

55. Liu, Y., Xu, R., Gu, H., Zhang, E., Qu, J., Cao, W., Huang, X., Yan, H., He, J., and Cai, Z. (2021). Metabolic reprogramming in macrophage responses. Biomark. Res. 9, 1. https://doi.org/10.1186/s40364-020-00251-y.

56. Mills, E.L., Kelly, B., Logan, A., Costa, A.S.H., Varma, M., Bryant, C.E., Tourlomousis, P., Däbritz, J.H.M., Gottlieb, E., Latorre, I., et al. (2016). Succinate dehydrogenase supports metabolic repurposing of mitochondria to drive inflammatory macrophages. Cell 167, 457–470.e13. https://doi.org/10.1016/j.cell.2016.08.064.

57. Wang, F., Zhang, S., Vuckovic, I., Jeon, R., Lerman, A., Folmes, C.D., Dzeja, P.P., and Herrmann, J. (2018). Glycolytic stimulation is not a requirement for M2 macrophage differentiation. Cell Metab. 28, 463–475.e4. https://doi.org/10.1016/j.cmet.2018.08.012.

58. Rando, T.A., and Jones, D.L. (2021). Regeneration, rejuvenation, and replacement: turning back the clock on tissue aging. Cold Spring Harb. Perspect. Biol. 13, a040907. https://doi.org/10.1101/cshperspect.a040907.

59. Hwang, J., Huang, Y., Burwell, T.J., Peterson, N.C., Connor, J., Weiss, S.J., Yu, S.M., and Li, Y. (2017). In situ imaging of tissue remodeling with collagen hybridizing peptides. ACS Nano 11, 9825–9835. https://doi.org/10.1021/acsnano.7b03150.

60. Kanisicak, O., Khalil, H., Ivey, M.J., Karch, J., Maliken, B.D., Correll, R.N., Brody, M.J., J Lin, S.C.J., Aronow, B.J., Tallquist, M.D., et al. (2016). Genetic lineage tracing defines myofibroblast origin and function in the injured heart. Nat. Commun. 7, 12260. https://doi.org/10.1038/ncomms12260.

61. Derrick, C.J., and Noël, E.S. (2021). The ECM as a driver of heart development and repair. Development 148, dev191320. https://doi.org/10.1242/dev.191320.

62. Tzahor, E., and Dimmeler, S. (2022). A coalition to heal-the impact of the cardiac microenvironment. Science 377, eabm4443. https://doi.org/10.1126/science.abm4443.

63. Hu, B., Lelek, S., Spanjaard, B., El-Sammak, H., Simões, M.G., Mintcheva, J., Aliee, H., Schäfer, R., Meyer, A.M., Theis, F., et al. (2022). Origin and function of activated fibroblast states during zebrafish heart regeneration. Nat. Genet. 54, 1227–1237. https://doi.org/10.1038/s41588-022-01129-5.

64. Jin, S., Guerrero-Juarez, C.F., Zhang, L., Chang, I., Ramos, R., Kuan, C.H., Myung, P., Plikus, M.V., and Nie, Q. (2021). Inference and analysis of cell-cell communication using CellChat. Nat. Commun. 12, 1088. https://doi.org/10.1038/s41467-021-21246-9.

65. Yokota, T., McCourt, J., Ma, F., Ren, S., Li, S., Kim, T.-H., Kurmangaliyev, Y.Z., Nasiri, R., Ahadian, S., Nguyen, T., et al. (2020). Type V collagen in scar tissue regulates the size of scar after heart injury. Cell 182, 545–562.e23. https://doi.org/10.1016/j.cell.2020.06.030.

66. Izu, Y., Adams, S.M., Connizzo, B.K., Beason, D.P., Soslowsky, L.J., Koch, M., and Birk, D.E. (2021). Collagen XII mediated cellular and extracellular mechanisms regulate establishment of tendon structure and function. Matrix Biol. 95, 52–67. https://doi.org/10.1016/j.matbio.2020.10.004.

67. Herz, J., Goldstein, J.L., Strickland, D.K., Ho, Y.K., and Brown, M.S. (1991). 39-kDa protein modulates binding of ligands to low density lipoprotein receptor-related protein/alpha 2-macroglobulin receptor. J. Biol. Chem. 266, 21232–21238.

68. Wehner, D., Tsarouchas, T.M., Michael, A., Haase, C., Weidinger, G., Reimer, M.M., Becker, T., and Becker, C.G. (2017). Wnt signaling controls pro-regenerative Collagen XII in functional spinal cord regeneration in zebrafish. Nat. Commun. 8, 126. https://doi.org/10.1038/s41467-017-00143-0.

69. Schönborn, K., Willenborg, S., Schulz, J.-N., Imhof, T., Eming, S.A., Quondamatteo, F., Brinckmann, J., Niehoff, A., Paulsson, M., Koch, M., et al. (2020). Role of collagen XII in skin homeostasis and repair. Matrix Biol. 94, 57–76. https://doi.org/10.1016/j.matbio.2020.08.002.

70. Yamamoto, K., Okano, H., Miyagawa, W., Visse, R., Shitomi, Y., Santamaria, S., Dudhia, J., Troeberg, L., Strickland, D.K., Hirohata, S., et al. (2016). MMP-13 is constitutively produced in human chondrocytes and co-endocytosed with ADAMTS-5 and TIMP-3 by the endocytic receptor LRP1. Matrix Biol. 56, 57–73. https://doi.org/10.1016/j.matbio.2016.03.007.

71. Lillis, A.P., Van Duyn, L.B., Murphy-Ullrich, J.E., and Strickland, D.K. (2008). LDL receptor-related protein 1: unique tissue-specific functions revealed by selective gene knockout studies. Physiol. Rev. 88, 887–918. https://doi.org/10.1152/physrev.00033.2007.

72. Gonias, S.L., and Campana, W.M. (2014). LDL receptor-related protein-1: a regulator of inflammation in atherosclerosis, cancer, and injury to the nervous system. Am. J. Pathol. 184, 18–27. https://doi.org/10.1016/j.ajpath.2013.08.029.

73. Cunningham, F., Allen, J.E., Allen, J., Alvarez-Jarreta, J., Amode, M.R., Armean, I.M., Austine-Orimoloye, O., Azov, A.G., Barnes, I., Bennett, R., et al. (2022). Ensembl 2022. Nucleic Acids Res. 50, D988–D995. https://doi.org/10.1093/nar/gkab1049.

74. Satija, R., Farrell, J.A., Gennert, D., Schier, A.F., and Regev, A. (2015). Spatial reconstruction of single-cell gene expression data. Nat. Biotechnol. 33, 495–502. https://doi.org/10.1038/nbt.3192.

75. Yu, G., Wang, L.G., Han, Y., and He, Q.Y. (2012). ClusterProfiler: an R package for comparing biological themes among gene clusters. Omics 16, 284–287. https://doi.org/10.1089/omi.2011.0118.

76. Wu, T., Hu, E., Xu, S., Chen, M., Guo, P., Dai, Z., Feng, T., Zhou, L., Tang, W., Zhan, L., et al. (2021). clusterProfiler 4.0: A universal enrichment tool for interpreting omics data. Innovation (Camb) 2, 100141. https://doi.org/10.1016/j.xinn.2021.100141.

77. Finak, G., McDavid, A., Yajima, M., Deng, J., Gersuk, V., Shalek, A.K., Slichter, C.K., Miller, H.W., McElrath, M.J., Prlic, M., et al. (2015). MAST: A flexible statistical framework for assessing transcriptional changes and characterizing heterogeneity in single-cell RNA sequencing data. Genome Biol. *16*, 278. https://doi.org/10.1186/s13059-015-0844-5.

78. Wolf, F.A., Angerer, P., and Theis, F.J. (2018). SCANPY: large-scale single-cell gene expression data analysis. Genome Biol. *19*, 15. https://doi.org/10.1186/s13059-017-1382-0.

79. Wolf, F.A., Hamey, F.K., Plass, M., Solana, J., Dahlin, J.S., Göttgens, B., Rajewsky, N., Simon, L., and Theis, F.J. (2019). PAGA: graph abstraction reconciles clustering with trajectory inference through a topology preserving map of single cells. Genome Biol. *20*, 59. https://doi.org/10.1186/s13059-019-1663-x.

80. Bergen, V., Lange, M., Peidli, S., Wolf, F.A., and Theis, F.J. (2020). Generalizing RNA velocity to transient cell states through dynamical modeling. Nat. Biotechnol. *38*, 1408–1414. https://doi.org/10.1038/s41587-020-0591-3.

81. La Manno, G., Soldatov, R., Zeisel, A., Braun, E., Hochgerner, H., Petukhov, V., Lidschreiber, K., Kastriti, M.E., Lönnerberg, P., Furlan, A., et al. (2018). RNA velocity of single cells. Nature *560*, 494–498. https://doi.org/10.1038/s41586-018-0414-6.

82. Schindelin, J., Arganda-Carreras, I., Frise, E., Kaynig, V., Longair, M., Pietzsch, T., Preibisch, S., Rueden, C., Saalfeld, S., Schmid, B., et al. (2012). Fiji: an open-source platform for biological-image analysis. Nat. Methods *9*, 676–682. https://doi.org/10.1038/nmeth.2019.

83. Mickoleit, M., Schmid, B., Weber, M., Fahrbach, F.O., Hombach, S., Reischauer, S., and Huisken, J. (2014). High-resolution reconstruction of the beating zebrafish heart. Nat. Methods *11*, 919–922. https://doi.org/10.1038/nmeth.3037.

84. Gray, C., Loynes, C.A., Whyte, M.K.B., Crossman, D.C., Renshaw, S.A., and Chico, T.J.A. (2011). Simultaneous intravital imaging of macrophage and neutrophil behaviour during inflammation using a novel transgenic zebrafish. Thromb. Haemost. *105*, 811–819. https://doi.org/10.1160/TH10-08-0525.

85. Davison, J.M., Akitake, C.M., Goll, M.G., Rhee, J.M., Gosse, N., Baier, H., Halpern, M.E., Leach, S.D., and Parsons, M.J. (2007). Transactivation from Gal4-VP16 transgenic insertions for tissue-specific cell labeling and ablation in zebrafish. Dev. Biol. *304*, 811–824. https://doi.org/10.1016/j.ydbio.2007.01.033.

86. Thiele, T.R., Donovan, J.C., and Baier, H. (2014). Descending control of swim posture by a midbrain nucleus in zebrafish. Neuron *83*, 679–691. https://doi.org/10.1016/j.neuron.2014.04.018.

87. Ham, T.J. van, Mapes, J., Kokel, D., and Peterson, R.T. (2010). Live imaging of apoptotic cells in zebrafish. FASEB J. *24*, 4336–4342. https://doi.org/10.1096/fj.10-161018.

88. Cao, J., and Poss, K.D. (2016). Explant culture of adult zebrafish hearts for epicardial regeneration studies. Nat. Protoc. *11*, 872–881. https://doi.org/10.1038/nprot.2016.049.

89. Apaydin, D.C., Jaramillo, P.A.M.M., Corradi, L., Cosco, F., Rathjen, F.G., Kammertoens, T., Filosa, A., and Sawamiphak, S. (2020). Early-life stress regulates cardiac development through an IL-4-glucocorticoid signaling balance. Cell Rep. *33*, 108404. https://doi.org/10.1016/j.celrep.2020.108404.

STAR★METHODS

KEY RESOURCES TABLE

REAGENT or RESOURCE	SOURCE	IDENTIFIER
Antibodies		
Rabbit anti-MEF-2 Antibody (C-21)	Santa Cruz	Cat#sc-313; RRID: AB_631920
Rat anti-mCherry Antibody (16D7)-100µl	LIFE Technologies	Cat#M11217; RRID: AB_2536611
Mouse anti-PCNA antibody [PC10]	Abcam	Cat#ab18197; RRID: AB_444313
Chicken anti-GFP antibody	LIFE Technologies	Cat#A10262; RRID: AB_2534023
Goat anti-Chicken IgY (H+L) Secondary Antibody, Alexa Fluor 488	LIFE Technologies	Cat#A11039; RRID: AB_2534096
Goat Anti-rat IgG (H+L), (Alexa Fluor(R) 555 Conjugate)	Cell Signaling	Cat#4417S; RRID: AB_10696896
Rabbit anti-cd31 antibody	Abcam	Cat#ab28364; RRID: AB_726362
Rabbit anti-Collagen I antibody	Abcam	Cat#ab233639; RRID: AB_3068540
Mouse anti-alpha smooth muscle Actin antibody [1A4]	Abcam	Cat#ab7817; RRID: AB_262054
Mouse anti-Tubulin, Acetylated antibody [6-11B-1]	Sigma	Cat#T6793; RRID: AB_477585
Mouse anti-TNF alpha antibody [52B83]	Abcam	Cat#ab1793; RRID: AB_302615
Rabbit anti-Col1a1a antibody	GeneTex	Cat#GTX133063; RRID: AB_2886813
Goat anti-mouse IgG (H+L), (Alexa Fluor(R) 488 Conjugate)	Cell Signaling	Cat#4408S; RRID: AB_10694704
Goat anti-mouse IgG (H+L), F(ab')2 Fragment (Alexa Fluor(R) 647 Conjugate)	Cell Signaling	Cat#4410S; RRID: AB_1904023
Goat anti-rabbit IgG (H+L),(Alexa Fluor(R) 488 Conjugate)	Cell Signaling	Cat#4412S; RRID: AB_1904025
Bacterial and virus strains		
NEB 5-alpha Competent E. coli (High Efficiency)	NEB	Cat#C2987H
Chemicals, peptides, and recombinant proteins		
Collagen Hybridizing Peptide, 5-FAM Conjugate	3-Helix	Cat#FLU300 / FLU60
recombinant zebrafish LRPAP1 protein	This paper	
carvedilol	Sigma	Cat#3993
(±)-Propranolol hydrochloride	Sigma	Cat#P0884
Atropine sulfate salt monohydrate	Sigma	Cat#A0257
Prazosin hydrochloride	Sigma	Cat#P7791
Methoxamine hydrochloride	Sigma	Cat#M6524
5-Ethynyl-2′-deoxyuridine (EdU)	Santa Cruz	Cat#61135-33-9
Dulbecco's Modified Eagle Medium, high glucose, GlutaMAX	GIBCO	Cat#31966021
Fetal Bovine Serum	GIBCO	Cat#10270106
MEM Non-Essential Amino Acids Solution (100X)	Thermo Fisher	Cat#11140050
Penicillin-Streptomycin (10.000 U/ml)	Thermo Fisher	Cat#15140122
Fibronectin Bovine Protein, Plasma	Thermo Fisher	Cat#33010-018
Primocin	InvivoGen	Cat#ant-pm-2
2-Mercaptoethanol	Sigma	Cat#M3148
Aniline Blue	Santa Cruz	Cat#28631-66-5
Acid fuchsin	Carl Roth	Cat#T128.1
Orange G	Santa Cruz	Cat#1936-15-8
Entellan	Sigma	Cat#1.07960
Fluoromount Aqueous Mounting Medium	Sigma	Cat#F4680
HCR™ IF + HCR™ RNA-FISH Products	Molecular Instruments	
Chromium Next GEM Single Cell 3' GEM, Library & Gel Bead Kit v3.1	10x Genomics	Cat#PN-1000121
Chromium Next GEM Chip G Single Cell Kit	10x Genomics	Cat#PN-1000120

Continued

REAGENT or RESOURCE	SOURCE	IDENTIFIER
Single Index Kit T Set A	10x Genomics	Cat#PN-1000213
Qubit dsDNA HS Assay Kit	LIFE Technologies	Cat#Q32851
DAPI staining solution for FACS	Milteny Biotec	Cat#130-111-570
DAPI	Sigma	Cat#D9542-5MG
LIBERASE TL RESEARCH GRADE 10 MG	Sigma	Cat#05401020001
In-Fusion® Snap Assembly Master Mix	Takara-Bio	Cat#638948
PLURONIC F-68(R) POLYOL	Th. Geyer	Cat#2750049
Critical commercial assays		
IP3(Inositol Triphosphate) ELISA Kit	Biocat	Cat#E-EL-0059-ELS
Click-iT Plus EdU Alexa Fluor 647 Imaging Kit-1 kit	LIFE Technologies	Cat#C10640
Morphine	Ratiopharm	N/A
Tricaine	PHARMAQ	N/A
Deposited data		
adult *csf1ra:Gal4; UAS:NTR-mCherry zebrafish hearts* (processed and raw scRNA-seq data)	This paper	GEO: GSE205103
adult *csf1ra:Gal4; UAS:adra1-3i-T2A-CFP; UAS:NTR-mCherry* zebrafish hearts (processed and raw scRNA-seq data)	This paper	GEO: GSE205103
Experimental models: Organisms/strains		
Zebrafish: *Tg(myl7:H2B-GFP)*[zf521]	Huisken lab, Max Planck Institute of Molecular Cell Biology and Genetics	ZDB-ALT-150204-1
Zebrafish: *TgBAC(csf1ra:Gal4-VP16)*[i186]	Chico Lab, Centre for Biomedical and Developmental Genetics	ZDB-ALT-110707-2
Zebrafish: *Tg(UAS:NTR-mCherry)*[c264]	Zebrafish International Resource Center	ZDB-ALT-070316-1
Zebrafish: *Tg(14xUAS:GCaMP6s)*[mpn101]	Baier Lab, Max Planck Institute of Neurobiology Department Genes – Circuits – Behavior	ZDB-ALT-140811-3
Zebrafish: *Tg(tbp:Gal4,myl7:Cerulean)*[f13]	Zebrafish International Resource Center	ZDB-ALT-110328-4
Zebrafish: *Tg(tnfa:EGFPF)*[ump5]	European Zebrafish Resource Center	ZDB-ALT-151130-3
Zebrafish: *Tg(UAS:adra1-3i-T2A-CFP)* [m81]	This paper	N/A
Oligonucleotides		
See Table S1 for all primers	This paper	N/A
Software and algorithms		
Graphpad Prism 8.0	GraphPad Software, San Diego, California USA, www.graphpad.com	RRID:SCR_002798
Seurat package v4.1.0[74]	https://satijalab.org/seurat/get_started.html	RRID:SCR_016341
clusterProfiler package v4.6.2[75,76]	http://bioconductor.org/packages/release/bioc/html/clusterProfiler.html	RRID:SCR_016884
CellChat package v1.6.1[64]	https://github.com/sqjin/CellChat	RRID:SCR_021946
MAST package v1.24.1[77]	https://bioconductor.org/packages/release/bioc/html/MAST.html	RRID:SCR_016340
scanpy v1.9.1[78,79]	https://github.com/theislab/scanpy	RRID:SCR_018139
scvelo v0.2.5[80]	https://github.com/theislab/scvelo	RRID:SCR_018168
Velocyto[81]	http://velocyto.org/	RRID:SCR_018167
Imaris 9.5.0	Oxford Instruments	RRID:SCR_007370
Fiji[82]	http://fiji.sc	RRID:SCR_002285

RESOURCE AVAILABILITY

Lead contact
Further information and requests for resources and reagents should be directed to and will be fulfilled by the lead contact, Dr. Suphansa Sawamiphak (suphansa.sawamiphak@mdc-berlin.de)

Materials availability
The zebrafish line *(UAS:NTR-mCherry; UAS:adra1-3i-T2A-CFP)* and zebrafish Lrpap1 protein generated here are available upon request.

Data and code availability
Single-cell RNA-seq data have been deposited at GEO and are publicly available. Accession numbers are listed in the key resources table. This paper does not report original code. Any additional information required to reanalyze the data reported in this paper is available from the lead contact upon request.

EXPERIMENTAL MODEL AND STUDY PARTICIPANT DETAILS

Animal care and strains
Zebrafish husbandry and experimental treatments were performed under institutional (Max Delbrück Center for Molecular Medicine), State (LAGeSo Berlin), and German ethical and animal welfare guidelines. Zebrafish were kept under standard conditions at 28.5°C on a 14 hr/10 hr light/dark cycle. Embryos and larvae were raised in Danieau's medium (58 mM NaCl, 0.7 mM KCl, 0.4 mM MgSO4, 0.6 mM Ca(NO3), 2,5 mM HEPES, pH adjusted to 7). Sex of the zebrafish were not discriminated. Adult zebrafish used in the study were 1 to 2 years old whereas larval zebrafish were either 5 dpf or 7 dpf as stated in the experimental details. Previously generated transgenic lines used in this study are *Tg(myl7:H2B-GFP)^{zf521}*,[83] *TgBAC(csf1ra:Gal4-VP16)^{i186}*,[84] *Tg(UAS:NTR-mCherry)^{c264}*,[85] *Tg(14xUAS:GCaMP6s)^{mpn101}*,[86] *Tg(tbp:Gal4,myl7:Cerulean)^{f13}*,[87] *Tg(tnfa:EGFPF)^{ump5}*.[52] Phenylthiourea (PTU) was used when relevant, starting from 1 dpf to block zebrafish skin pigmentation.

METHOD DETAILS

Generation of expression constructs and transgenic animals
The *UAS:adra1-3i-T2A-CFP* construct was generated by cloning the sequence coding for the 3rd intracellular loop of *adra1bb*, corresponding to the amino acids from 231 to 291, the T2A self-cleaving peptide and CFP, downstream of 14XUAS regulatory element in a pTol2 vector. Cloning was done by In-Fusion® HD Cloning Plus kit (Takara-Bio) according to the instructions of the manufacturer. Generation of the *Tg(UAS:adra1-3i-T2A-CFP)^{m81}* line was obtained by injecting the *UAS:adra1-3i-T2A-CFP* construct together with mRNA encoding the Tol2 transposase in to embryos at 1-cell stage. Founders with stable integration of the transgene were identified and outcrossed to expand the offspring.

Imaging
A Zeiss LSM 880 confocal microscope and Leica DM6 CFS confocal microscope were used for imaging live or fixed samples. For AFOG staining imaging, an Olympus SZX16 stereo microscope was used. For live imaging, zebrafish larvae were mounted in 1.5% low-melting agarose (EURx) in petri dishes.

Heart injury
For larvae, a two-photon laser was used to induce a focal injury in the ventricle. Larvae were anesthetized with tricaine and mounted in 1.5% low-melting agarose in petri dishes filled with Danieau's medium. Part of the agarose covering the heart was removed. Five pulses of 920 nm laser, each approximately 0.8 ms long, were applied to the ventricle with a W Plan-APOCHROMAT 20x/1.0 DIC (UV) VIS-IR dipping lens (Zeiss). The larvae were then removed from agarose and released into Danieau's medium.

Adult zebrafish anesthetized in Danieau's medium containing 0.168 mg/ml tricaine were first stabilized on a sponge with a small groove soaked in the same medium. A small incision was made in the body wall and the pericardium to expose the heart. The ventricular apex was then touched with the tip of a cryoprobe, pre-frozen by immersion in liquid nitrogen, until thawed. Subsequently, fish were released into system water containing 1.5 μg/ml morphine (Ratiopharm). At 6 hpi, the morphine-containing water was replaced with system water and fish were left to recover in regular rearing conditions or proceed to pharmacological treatment for up to 7 dpi.

Pharmacological treatments
Zebrafish larvae were treated with neurotransmitter blockers after two-photon laser injury for 24 h. Drugs were administered in Danieau's solution at the following concentrations; carvedilol (Sigma) at 50 μM, propranolol (Sigma) at 50 μM, atropine (Sigma) at 50 μM, and prazosin (Sigma) at 100 μM. Control groups were treated with solvents of the drugs in equal volume as vehicle. For assessment of cell proliferation, 500 μM 5-Ethynyl-2'-deoxyuridine (EdU) (Santa Cruz) was added to the medium at 6 hpi. After the incubation period

the larvae were anesthetized with tricaine, culled, and fixed with 4% PFA + 0.03% TritonX-100 (Sigma) at 4°C overnight. For adult zebrafish treatment, prazosin, was administered in system water at 100 μM, after the injury up to 7 dpi. Prazosin-containing water was replaced daily.

Heart dissection and cryosectioning
Adult zebrafish were culled by incubating in ice water at 0-4°C for at least 20 min to induce hypothermia. Hearts were then collected following decapitation from the base of pectoral fin with a razor blade and fixed in 4% PFA + 0.03% TritonX-100 at 4°C overnight. After washing with PBS containing 0.1% (V/V) TritonX-100 (PBST), hearts were kept in methanol at -20°C for long term storage or at least overnight before proceeding to other steps. For cryosectioning, hearts were rehydrated in gradually reduced concentration of methanol solutions diluted in PBS and finally washed in PBS. Subsequently, they were submerged in 15% sucrose solution for 3–5 h, then in 30% sucrose solution overnight for cryopreservation. Hearts were mounted in molds filled with OCT (Sakura) and stored at -80°C. 10 μm cryosections from the frozen hearts were collected for histological analysis and immunofluorescent staining.

Tissue dissociation
Tissues were transferred into dissociation solution containing 0.26 U/ml LiberaseTM enzyme mixture (Sigma) and 1X Pluronic F-68 (ThermoFisher) in HBSS, and then incubated in dissociation solution for 30 min with shaking at 750 rpm at 37°C with intermittent pipetting (every 5 min). The dissociation reaction was stopped by addition of an equal volume of 1% BSA in HBSS, followed by cell pelleting and centrifugation at 200xg at 4°C. Cells were washed with 0.05% BSA in HBSS solution, resuspended in this solution and filtered with a 40 μm cell strainer.

Production of recombinant Lrpap1
The sequence of zebrafish Lrpap1 was obtained from the UniProt protein database under accession number Q7ZW96. The gene sequence was synthesized and cloned into a pET-24(+) expression vector, under transcriptional control of the T7 promoter. The plasmid was transfected into Escherichia coli, and the recombinant protein was purified from bacteria using a 6xHis affinity tag. The histidine tag was removed by TEV protease after the purification. The size and mass of the protein were confirmed by SDS-PAGE gel and liquid chromatography/time-of-flight mass spectrometry (LC/MS TOF).

Explant culture and cryoinjury
Zebrafish were culled as explained above and instead of fixation, hearts were washed with phosphate-buffered saline (PBS). Hearts were cultured according to a previously published protocol,[88] briefly they were placed in explant medium (DMEM, 10% FBS, 1% MEM-NEAA, 100 U/ml penicillin, 100 ug/ml streptomycin, 100 ug/ml primocin, 50 uM 2-mercaptoethanol) in a 24-well culture plates and incubated at 28 °C in a cell culture incubator. For ex vivo cryoinjury, the hearts were transferred to an empty petri dish, extra medium around the hearts was carefully removed and then a precooled cryoprobe was applied to the ventricular wall for 20 s. All the hearts were transferred to the fresh explant medium in 24-well culture plates after cryoinjury and the plates were placed in a cell culture incubator at 28 °C for 7 days. LRPAP1 (10 μg/μl) was added to the medium from the first day of cryoinjury. 500 uM methoxamine was added from the fourth day after the injury until the seventh day to provide activation of α1 adrenergic receptors, which otherwise would be absent in the explanted hearts. Explant medium, LRPAP1, and methoxamine were refreshed daily after their respective addition times.

ELISA
Tg(tbp:Gal4, myl7:Cerulean)^f13; Tg(UAS:adra1-3i-T2A-CFP) and *Tg(tbp:Gal4, myl7:Cerulean)^f13* (control) 5 dpf larvae were treated with vehicle, 200 μM methoxamine (Sigma) or 100 μM prazosin (Sigma). Wild type 5 dpf larvae were treated with 50 μM carvedilol (Sigma) only, 200 μM methoxamine (Sigma) only, combination of both or vehicle. After treatments, IP3 levels were measured with Elabscience IP3 ELISA kit according to the manufacturer's instructions. Briefly, larvae were pooled and dissociated according to our explained dissociation protocol. Then cells were lysed with an ultrasonic cell disruptor and centrifuged 10 min at 5000xg at 4 °C and supernatants were collected. Then standards supplied with the kit and our samples were added to the ELISA plate wells, and Biotinylated detection antibody solution and HRP conjugate working solutions, supplied with the kit, were added. A Tecan Spark 20m plate reader was used to measure the signal intensities of the samples after incubation times indicated by the manufacturer's protocol.

Calcium measurement
TgBAC(csf1ra:Gal4); Tg(UAS:NTR-mCherry); Tg(UAS:adra1-3i-T2A-CFP; Tg(14xUAS:GCaMP6s) larvae were mounted in 1.5% low-melting agarose (EURx). Baseline calcium signal in CFP⁻ and CFP⁺ macrophages in the same larvae was imaged every 0.2 seconds for 3 min. 200 mM methoxamine (Sigma) was then added, and larvae were continually imaged at the same frequency for 10 min. GCaMP6s fluorescence was measured with ImageJ[82] by manually selecting macrophages (mCherry⁺ and GCaMP6s ⁺ cells) either positive or negative for CFP as regions of interest. Then $\Delta F/F_0$ $((F - F_0)/F_0)$, where F_0 is the average fluorescence intensity at baseline and F is average fluorescence intensity after methoxamine addition, were calculated for individual cells.

Immunofluorescence and histological staining

For immunostaining of larvae, a previously described protocol for whole mount larvae staining was used.[89] Briefly, after fixation, samples were gradually switched to 100% methanol and incubated overnight at -20 °C. Then gradually switched back to PBST. If the samples were not treated with PTU, at this stage they were treated with 3% H2O2 + 0.5% KOH for 30 min RT on a rotator to remove skin pigment, and rinsed with PBST again. Antigen retrieval step was applied by incubating the samples in 150 mM tris pH 5.0 for 5 min in RT and at 70 ℃ with 600rpm shaking for 15 min. Samples were permeabilized with 1:20 diluted Trypsin-EDTA (500 BAEE units, Sigma) in PBST for 35 min. Then they were incubated in blocking solution containing 5% (v/v) goat serum and 1% (w/v) BSA in PBS for 1 h at RT, and then in primary antibody solutions (antibodies diluted in blocking solution) for 3 days at 4 ℃, followed by secondary antibody solutions (in blocking solution) for 3 days at 4 ℃ protected from light. The following primary antibodies were used for larval zebrafish staining: rat anti-mCherry (1:300, ThermoFisher), chick anti-GFP (1:500, ThermoFisher). The following secondary antibodies were used for larval zebrafish staining: Alexa Fluor 488 anti-chicken (1:1000, ThermoFisher), Alexa Fluor 555 anti-rat (1:500, Cell Signaling). DAPI (1:300, Sigma) was added during the secondary antibody incubations. For EdU staining following the immunofluorescence staining, the Click-iT™ Plus EdU Cell Proliferation Kit Alexa 647 (ThermoFisher) was used according to manufacturer's instructions after the permeabilization step in the protocol. Stained larvae were mounted in Fluoromount aqueous mounting medium (Sigma) for imaging.

For immunostaining on adult cryosections, first the sections were fixed in ice-cold acetone (Sigma) at -20°C for 10 min and washed 3 times with PBS. Tissues were then permeabilized with 0.2% TritonX-100 in PBS for 10 min, and washed 3 times with PBS. Sections were blocked with blocking solution containing 5% (v/v) goat serum and 10% (w/v) BSA in PBS. Appropriate primary antibodies diluted in the blocking solution were then incubated with the sections at 4°C overnight and washed 3 times with PBS containing 0.3% Tween20. Subsequently, secondary antibodies were added to the sections and incubated at 4°C overnight. If needed, DAPI (Sigma) was added during the secondary antibody incubation. Then sections were washed with PBS 3 times and mounted with Fluoromount aqueous mounting medium (Sigma) for imaging. The following primary antibodies were used: rabbit anti-Mef2 (1:300, Santa Cruz), mouse anti-PCNA (1:300, Abcam), rabbit anti-CD31 (1:300, Abcam), rabbit anti-Col1 (1:300, Abcam), mouse anti-a-SMA (1:150, Abcam), mouse anti-acTub (1:300, Sigma), rat anti-mCherry (1:300, ThermoFisher), chick anti-GFP (1:500, ThermoFisher), mouse anti-Tnfa (1:200, Abcam), rabbit anti-col1a1a (GeneTex). The following secondary antibodies were used: Alexa Fluor 488 anti-chicken (1:1000, ThermoFisher), Alexa Fluor 555 anti-rat (1:500, Cell Signaling), Alexa Fluor 647 anti-mouse (1:500, Cell Signaling), Alexa Fluor 488 anti-mouse (1:500, Cell Signaling), Alexa Fluor 647 anti-rabbit (1:500, Cell Signaling), Alexa Fluor 488 anti-rabbit (1:500, Cell Signaling). For CHP (Tebu-bio) staining, CHP was heated at 80°C for 5 min and quenched to room temperature (RT) in ice water quickly before using it according to manufacturer's instructions. Briefly, following the immuno-staining protocol up to the secondary antibody step, 30 μM of CHP solution was added to samples together with secondary antibodies. Samples were incubated at 4°C overnight, washed 3 times with PBS, and finally mounted with Fluoromount aqueous mounting medium (Sigma) for imaging.

Acid Fuchsin Orange G (AFOG) staining

Cryosections were fixed in Bouin's solution for 2 h at 58°C and 1 h at RT and washed with running tap water for 20 min. Then tissues were covered with 1% phosphomolybdic acid and 0.25% phosphotungstic acid solution for 5 min and washed with deionized water for 5 min. Sections were then incubated for 5 min with AFOG solution containing 1g Aniline Blue (Santa Cruz), 3g acid Fuchsin (Roth), 2g Orange G (Santa Cruz) in distilled water (pH adjusted to 1.1). After washing with distilled water for 5 min, sections were dehydrated in consecutive ethanol (3 times) and xylene (3 times) baths and mounted with Entellan (Merck Millipore).

Hybridization chain reaction (HCR) and fluorescent in situ hybridization (FISH)

mRNA expression of *postnb, col12a1a, cxcl12b, lrp1aa, mdka, lyve1, col5a1, sdc2* were assessed, following immunofluorescent staining for detection of other proteins as described earlier, by HCR RNA fluorescence in situ hybridization (HCR RNA-FISH) according to the manufacturer's protocol (Molecular Instruments). Probe hybridization buffer, amplification buffer, wash buffer and hairpins were provided by the manufacturer. After immunofluorescent labelling, sections were post-fixed with 4% PFA for 10 mins at RT, washed twice with PBS containing 0.1% (V/V) Tween 20 for 5 mins each, and once with 5x SSCT solution containing sodium chloride sodium citrate (SSC) and 0.1% (V/V) Tween 20 at RT for 5 min. Sections were then incubated with probe hybridization buffer for 10 mins at 37°C followed by overnight incubation at 37°C with 16 nM probe solution with the *postnb* probe. Subsequently, they were washed sequentially with the following solutions for 15 min each at 37°C: 75% of probe wash buffer / 25% 5× SSCT, 50% of probe wash buffer / 50% 5× SSCT, 25% of probe wash buffer / 75% 5× SSCT, and 100% 5× SSCT. Then sections were incubated at RT for 30 min with amplification buffer. Hairpins were snap cooled by first heating them at 95°C for 90 seconds and then cooling them to RT. Then sections were incubated overnight with amplification solution containing 60 nM of hairpin in the dark at RT. Subsequently, sections were washed with 5x SSCT 2 times for 5 min each, 2 times for 15 min each and 1 time for 5 min at RT. Then they were mounted with Fluoromount aqueous mounting medium (Sigma) for imaging.

Image analyses

To assess macrophage trafficking to the injured heart, we used the transgenic line *csf1ra:Gal4; UAS:NTR-mCherry; UAS:adra1-3i-CFP; tnfa:EGFPF*. Contribution of adra1 signaling-deficient (CFP⁺mCherry⁺), as compared to control (mCherry⁺) macrophages in the same larvae, to the *tnfa*⁺ (EGFPF⁺) and *tnfa*⁻ (EGFPF⁻) macrophage populations trafficked to the hearts at different time points after

laser-induced injury was quantified from confocal time series that traced macrophage dynamics for 24 h. At each time point indicated, numbers of these four macrophage pools localized within 100 μm distance from injury site were counted.

To quantify larval cardiomyocyte proliferation, nuclei showing H2B-GFP and EdU colocalization from all single-plane images in confocal stacks covering the entire cardiac ventricles were counted in ImageJ.[82] Total cardiomyocyte numbers were quantified with Imaris software (Oxford Instruments). Total macrophages and proliferating macrophages, labelled with NTR-mCherry and EdU, were similarly quantified from an area within 100 μm distance from injury border zone. Macrophages with *adra1-3i-T2A-CFP* and/or *tnfa* expression were counted according to the presence of CFP and/or GFP, with mCherry double positive signals from the reporter transgenes.

For adult heart sections, cell numbers were counted from inside the injury site and proximal area within 100 μm from the injury border zone. For all the sham operated hearts, a similar sized area around the ventricular apex was quantified. All quantifications were performed on at least 3 sections and averaged for each heart. Col1, CD31, acTub and CHP levels were assessed by thresholding the images and measuring the area covered by the respective signals in ImageJ.[82] Percentages of these areas in the injured hearts, or similar-sized areas around the apex for sham operated hearts, were then calculated. For collagen quantification from the AFOG staining, the ImageJ[82] color threshold tool was used to calculate percentage of collagen (blue) covered area inside the injury area or in a similar sized area around the apex for sham operated hearts. For HCR quantifications, areas of measurement were chosen as described above and cells positive for respective signals were counted. Signal intensity quantification of HCR staining was done with ImageJ[82] by measuring the integrated density of the signal and normalizing it by measurement area.

Fluorescent activated cell sorting (FACS)

Dissociated larvae or hearts were sorted with a BD FACSAria II machine. For single cell RNA sequencing, cells were stained with DAPI (Milteny Biotech) prior to sorting for separating live/dead cells. Cells were first gated with FSC-A vs SSC-A to account for cell size and granularity to exclude cellular debris and clumps. Then FSC-H vs FSC-W and SSC-H vs SSC-W plots were used to gate only single cells within physiologically expected size range. Cells that fell in to these gates in the first steps were included in the downstream gating strategies to either collect live cells or to investigate cells with mCherry or CFP signal. Gating mCherry or CFP signal was done by using the samples with no transgene (negative control) as a reference for background signal.

Single cell RNA sequencing and analyses

TgBAC(csf1ra:Gal4); Tg(UAS:NTR-mCherry); Tg(UAS:adra1-3i-T2A-CFP) zebrafish hearts and control *TgBAC(csf1ra:Gal4); Tg(UAS:NTR-mCherry)* zebrafish hearts subjected to cryoinjury were collected at 7 dpi and dissociated as explained above. Live cells were sorted by FACS and loaded into a Chromium 10x Genomics platform for single cell capture in droplets prior to library preparation following the Chromium Single Cell 3' Reagent Kits User Guide (v3.1 Chemistry) CG000204. Quantification of cDNA and library construction was done by Qubit dsDNA HS Assay Kit (Life Technologies) using a high-sensitivity DNA tape-station (Agilent). Sequencing was done with Illumina NovaSeq6000 system at 400 million reads per lane and paired-end 50 bp read length settings.

10x Genomics Cell Ranger software (v6.0.1) was used to perform alignment and custom reference genome assembly. The Danio_rerio.GRCz11 (release 104) version of the zebrafish genome was acquired from Ensembl database[73] and the CFP sequence was added to the reference genome, built by mkgtf function. For the control heart, the Danio_rerio.GRCz11 (release 104) version of the zebrafish genome was used for alignments. Subsequent analysis was carried out with R package Seurat[74] (4.1.0). Cells that had less than 200 genes and more than 2500 genes and cells that have more than 15% mitochondrial content were filtered out. We selected 2500 highly variable genes after regressing out the effects of total number of counts and the percentage of mitochondrial genes. Then they were log-transformed and scaled so that the data was zero-centered. Principal component analysis (PCA) was performed, and 20 components were kept. Clustering was done with Louvain algorithm in Seurat,[74] using default settings, with K-nearest neighbor graph of the remaining cells and a resolution of 1.0. t-Stochastic Neighbor Embedding (t-SNE) was then used for dimensionality reduction using 20 components. Following identification of differentially expressed genes (DEGs) for each cluster with Seurat by implementing MAST,[77] cells in clusters identified as monocytes/macrophages were used for downstream analysis involving macrophage/monocytes. These cells were separated into two subpopulations based on CFP expression and 2500 highly variable features were found again for each subpopulation with the same approaches, and data were scaled again. Clustering with 0.5 resolution and differential expression analysis were then performed on these two subpopulations. The same approach, except separation of macrophage/monocyte into two groups, was applied also to the control heart sample. Cells identified as fibroblasts were also taken as separate object during the analysis and up to differential expression analysis, the steps were applied again. Subclusters were identified based on the expression profile considering significantly upregulated genes compared to other clusters in the same group relying on literature. Heatmaps, scatter plots and violin plots were visualized by vlnPlot, doHeatmap and DimPlot functions in Seurat package. Gene ontology (GO) overrepresentation analysis (ORA) was performed with clusterProfiler package.[75,76] GO terms with more than 5 and less than 500 annotated genes from the DEG list were considered and filtered according to Bonferroni-Holm adjusted p values (0.05 cutoff).

The Cellchat[64] package was used for analyzing interactions between clusters of fibroblasts, macrophages and monocytes. Previously assigned cluster identities were used to label the clusters. Each cluster had more than 50 cells. Interaction numbers and their strength (weight) were plotted for all clusters first. Significant interactions between the 'ECM remodeling' macrophage/monocyte

cluster and other clusters were plotted with bubble representation in a table, and significant receptor-ligand pairs of interest for interactions between 'ECM remodeling', *col12a1a*[+] and perivascular cells clusters were plotted in chord diagrams.

RNA velocity analysis was done by using scanpy (v.1.9.1)[78,79] and scvelo (v.0.2.5),[80] and PAGA included in these modules were used for trajectory inference analysis. Velocity information for these analyses was obtained from reads mapped to Danio_rerio.GRCz11 (release 104) zebrafish genome using Cell Ranger software (v6.0.1) and velocyto.[81] The custom reference genome described above was used. Cell type identities assigned in previous steps were utilized again during velocity and trajectory inference analysis. Among the identified cell types, fibroblasts, macrophages, and monocytes were selected and then total counts were regressed out, number of genes and mitochondrial genes were filtered with similar parameters to previous steps and highly variable genes were found again. Then cells were re-clustered using similar parameters as before and PAGA analysis was run. RNA velocity values were calculated using default parameters for stochastic model of scvelo[80] module. These values were then plotted with UMAP representation of the dataset.

QUANTIFICATION AND STATISTICAL ANALYSIS

All data sets were first subjected to Shapiro-Wilk test to verify normal distribution. As all datasets were found to be normally distributed, statistical significance was determined using two-tailed Student's t tests in Graphpad Prism. The Fisher's F test was used to determine if the compared datasets had equal or unequal variance. In case of unequal variance, t tests with Welch's correction were performed. When performing multiple comparisons, p values were corrected using the Holm-Bonferroni method. Differences were considered statistically significant if $p < 0.05$. Statistical details including statistical test used, sample sizes, definition of center and dispersion are noted in the figures and figure legends. Softwares used for scRNAseq analysis are noted in the key resources table.